http://www.icact.org/journal.asp

ICACT-TACT JOURNAL

Transactions on Advanced Communications Technology

Volume 5 Issue 6, Nov. 2016, ISSN: 2288-0003

Editor-in-Chief
Prof. Thomas Byeongnam YOON, PhD.

GIRI Global IT Research Institute

Journal Editorial Board

■ Editor-in-Chief

■ Editors

Dr. Youssef SAID, Tunisie Telecom, Tunisia
Dr. Noor Zaman, King Faisal University, Al Ahsa Hofuf, Saudi Arabia
Dr. Srinivas Mantha, SASTRA University, Thanjavur, India
Dr. Shahriar Mohammadi, KNTU University, Iran
Prof. Beonsku An, Hongik University, korea
Dr. Guanbo Zheng, University of Houston, USA
Prof. Sangho Choe, The Catholic University of Korea, korea
Dr. Gyanendra Prasad Joshi, Yeungnam University, korea
Dr. Tae-Gyu Lee, Korea Institue of Industrial Technology(KITECH), korea
Prof. Ilkyeun Ra, University of Colorado Denver, USA
Dr. Yong Sun, Beijing University of Posts and Telecommunications, China
Dr. Yulei Wu, Chinese Academy of Sciences, China
Mr. Anup Thapa, Chosun University, korea
Dr. Vo Nguyen Quoc Bao, Posts and Telecommunications Institute of Technology, Vietnam
Dr. Harish Kumar, Bhagwant institute of technology, India
Dr. Jin REN, North china university of technology, China
Dr. Joseph Kandath, Electronics & Commn Engg, India
Dr. Mohamed M. A. Moustafa, Arab Information Union (AIU), Egypt
Dr. Mostafa Zaman Chowdhury, Kookmin University, Korea
Prof. Francis C.M. Lau, Hong Kong Polytechnic University, Hong Kong
Prof. Ju Bin Song, Kyung Hee University, korea
Prof. KyungHi Chang, Inha University, Korea
Prof. Sherif Welsen Shaker, Kuang-Chi Institute of Advanced Technology, China
Prof. Seung-Hoon Hwang, Dongguk University, Korea
Prof. Dal-Hwan Yoon, Semyung University, korea
Prof. Chongyang ZHANG, Shanghai Jiao Tong University, China
Dr. H K Lau, The Open University of Hong Kong, Honh Kong
Prof. Ying-Ren Chien, Department of Electrical Engineering, National Ilan University, Taiwan
Prof. Mai Yi-Ting, Hsiuping University of Science and Technology, Taiwan
Dr. Sang-Hwan Ryu, Korea Railroad Research Institute, Korea
Dr. Yung-Chien Shih, MediaTek Inc., Taiwan
Dr. Kuan Hoong Poo, Multimedia University, Malaysia
Dr. Michael Leung, CEng MIET SMIEEE, Hong Kong
Dr. Abu sahman Bin mohd Supa'at, Universiti Teknologi Malaysia, Malaysia
Prof. Amit Kumar Garg, Deenbandhu Chhotu Ram University of Science & Technology, India
Dr. Jens Myrup Pedersen, Aalborg University, Denmark
Dr. Augustine Ikechi Ukaegbu, KAIST, Korea
Dr. Jamshid Sangirov, KAIST, Korea
Prof. Ahmed Dooguy KORA, Ecole Sup. Multinationale des Telecommunications, Senegal
Dr. Se-Jin Oh, Korea Astronomy & Space Science Institute, Korea
Dr. Rajendra Prasad Mahajan, RGPV Bhopal, India
Dr. Woo-Jin Byun, ETRI, Korea
Dr. Mohammed M. Kadhum, School of Computing, Goodwin Hall, Queen's University , Canada
Prof. Seong Gon Choi, Chungbuk National University, Korea
Prof. Yao-Chung Chang, National Taitung University, Taiwan
Dr. Abdallah Handoura, Engineering school of Gabes - Tunisia, Tunisia
Dr. Gopal Chandra Manna, BSNL, India

Dr. Il Kwon Cho, National Information Society Agency, Korea
Prof. Jiann-Liang Chen, National Taiwan University of Science and Technology, Taiwan
Prof. Ruay-Shiung Chang, National Dong Hwa University, Taiwan
Dr. Vasaka Visoottiviseth, Mahidol University, Thailand
Prof. Dae-Ki Kang, Dongseo University, Korea
Dr. Yong-Sik Choi, Research Institute, IDLE co., ltd, Korea
Dr. Xuena Peng, Northeastern University, China
Dr. Ming-Shen Jian, National Formosa University, Taiwan
Dr. Soobin Lee, KAIST Institute for IT Convergence, Korea
Prof. Yongpan Liu, Tsinghua University, China
Prof. Chih-Lin HU, National Central University, Taiwan
Prof. Chen-Shie Ho, Oriental Institute of Technology, Taiwan
Dr. Hyoung-Jun Kim, ETRI, Korea
Prof. Bernard Cousin, IRISA/Universite de Rennes 1, France
Prof. Eun-young Lee, Dongduk Woman s University, Korea
Dr. Porkumaran K, NGP institute of technology India, India
Dr. Feng CHENG, Hasso Plattner Institute at University of Potsdam, Germany
Prof. El-Sayed M. El-Alfy, King Fahd University of Petroleum and Minerals, Saudi Arabia
Prof. Lin You, Hangzhou Dianzi Univ, China
Mr. Nicolai Kuntze, Fraunhofer Institute for Secure Information Technology, Germany
Dr. Min-Hong Yun, ETRI, Korea
Dr. Seong Joon Lee, Korea Electrotechnology Research Institute, korea
Dr. Kwihoon Kim, ETRI, Korea
Dr. Jin Woo HONG, Electronics and Telecommunications Research Inst., Korea
Dr. Heeseok Choi, KISTI(Korea Institute of Science and Technology Information), korea
Dr. Somkiat Kitjongthawonkul, Australian Catholic University, St Patrick's Campus, Australia
Dr. Dae Won Kim, ETRI, Korea
Dr. Ho-Jin CHOI, KAIST(Univ), Korea
Dr. Su-Cheng HAW, Multimedia University, Faculty of Information Technology, Malaysia
Dr. Myoung-Jin Kim, Soongsil University, Korea
Dr. Gyu Myoung Lee, Institut Mines-Telecom, Telecom SudParis, France
Dr. Dongkyun Kim, KISTI(Korea Institute of Science and Technology Information), Korea
Prof. Yoonhee Kim, Sookmyung Women s University, Korea
Prof. Li-Der Chou, National Central University, Taiwan
Prof. Young Woong Ko, Hallym University, Korea
Prof. Dimiter G. Velev, UNWE(University of National and World Economy), Bulgaria
Dr. Tadasuke Minagawa, Meiji University, Japan
Prof. Jun-Kyun Choi, KAIST (Univ.), Korea
Dr. Brownson ObaridoaObele, Hyundai Mobis Multimedia R&D Lab , Korea
Prof. Anisha Lal, VIT university, India
Dr. kyeong kang, University of technology sydney, faculty of engineering and IT , Australia
Prof. Chwen-Yea Lin, Tatung Institute of Commerce and Technology, Taiwan
Dr. Ting Peng, Chang'an University, China
Prof. ChaeSoo Kim, Donga University in Korea, Korea
Prof. kirankumar M. joshi, m.s.uni.of baroda, India
Dr. Chin-Feng Lin, National Taiwan Ocean University, Taiwan
Dr. Chang-shin Chung, TTA(Telecommunications Technology Association), Korea

Editor Guide

■ Introduction for Editor or Reviewer

All the editor group members are to be assigned as a evaluator(editor or reviewer) to submitted journal papers at the discretion of the Editor-in-Chief. It will be informed by eMail with a Member Login ID and Password.

Once logined the Website via the Member Login menu in left as a evaluator, you can find out the paper assigned to you. You can evaluate it there. All the results of the evaluation are supposed to be shown in the Author Homepage in the real time manner. You can also enter the Author Homepage assigned to you by the Paper ID and the author's eMail address shown in your Evaluation Webpage. In the Author Homepage, you can communicate each other efficiently under the peer review policy. Please don't miss it!

All the editor group members are supposed to be candidates of a part of the editorial board, depending on their contribution which comes from history of ICACT TACT as an active evaluator. Because the main contribution comes from sincere paper reviewing role.

■ Role of the Editor

The editor's primary responsibilities are to conduct the peer review process, and check the final camera-ready manuscripts for any technical, grammatical or typographical errors.

As a member of the editorial board of the publication, the editor is responsible for ensuring that the publication maintains the highest quality while adhering to the publication policies and procedures of the ICACT TACT(Transactions on the Advanced Communications Technology).

For each paper that the editor-in-chief gets assigned, the Secretariat of ICACT Journal will send the editor an eMail requesting the review process of the paper.

The editor is responsible to make a decision on an "accept", "reject", or "revision" to the Editor-in-Chief via the Evaluation Webpage that can be shown in the Author Homepage also.

■ Deadlines for Regular Review

Editor-in-Chief will assign a evalaution group(a Editor and 2 reviewers) in a week upon receiving a completed Journal paper submission. Evaluators are given 2 weeks to review the paper. Editors are given a week to submit a recommendation to the Editor-in-Chief via the evaluation Webpage, once all or enough of the reviews have come in. In revision case, authors have a maximum of a month to submit their revised manuscripts. The deadlines for the regular review process are as follows:

Evalution Procedure	Deadline
Selection of Evaluation Group	1 week
Review processing	2 weeks
Editor's recommendation	1 week
Final Decision Noticing	1 week

■ Making Decisions on Manuscript

Editor will make a decision on the disposition of the manuscript, based on remarks of the reviewers. The editor's recommendation must be well justified and explained in detail. In cases where the revision is requested, these should be clearly indicated and explained. The editor must then promptly convey this decision to the author. The author may contact the editor if instructions regarding amendments to the manuscript are unclear. All these actions could be done via the evaluation system in this Website. The guidelines of decisions for publication are as follows:

Decision	Description
Accept	An accept decision means that an editor is accepting the paper with no further modifications. The paper will not be seen again by the editor or by the reviewers.
Reject	The manuscript is not suitable for the ICACT TACT publication.
Revision	The paper is conditionally accepted with some requirements. A revision means that the paper should go back to the original reviewers for a second round of reviews. We strongly discourage editors from making a decision based on their own review of the manuscript if a revision had been previously required.

■ Role of the Reviewer

Reviewer Webpage:

Once logined the Member Login menu in left, you can find out papers assigned to you. You can also login the Author Homepage assigned to you with the paper ID and author's eMail address. In there you can communicate each other via a Communication Channel Box.

Quick Review Required:

You are given 2 weeks for the first round of review and 1 week for the second round of review. You must agree that time is so important for the rapidly changing IT technologies and applications trend. Please respect the deadline. Authors undoubtedly appreciate your quick review.

Anonymity:

Do not identify yourself or your organization within the review text.

Review:

Reviewer will perform the paper review based on the main criteria provided below. Please provide detailed public comments for each criterion, also available to the author.

- How this manuscript advances this field of research and/or contributes something new to the literature?
- Relevance of this manuscript to the readers of TACT?
- Is the manuscript technically sound?
- Is the paper clearly written and well organized?
- Are all figures and tables appropriately provided and are their resolution good quality?
- Does the introduction state the objectives of the manuscript encouraging the reader to read on?
- Are the references relevant and complete?

Supply missing references:

Please supply any information that you think will be useful to the author in revision for enhancing quality of the paperor for convincing him/her of the mistakes.

Review Comments:

If you find any already known results related to the manuscript, please give references to earlier papers which contain these or similar results. If the reasoning is incorrect or ambiguous, please indicate specifically where and why. If you would like to suggest that the paper be rewritten, give specific suggestions regarding which parts of the paper should be deleted, added or modified, and please indicate how.

Journal Procedure

Dear Author,

- **You can see all your paper information & progress.**

- **Step 1. Journal Full Paper Submission**

Using the Submit button, submit your journal paper through ICACT Website, then you will get new paper ID of your journal, and send your journal Paper ID to the Secretariat@icact.org for the review and editorial processing. Once you got your Journal paper ID, never submit again! Journal Paper/CRF Template

- **Step 2. Full Paper Review**

Using the evaluation system in the ICACT Website, the editor, reviewer and author can communicate each other for the good quality publication. It may take about 1 month.

- **Step 3. Acceptance Notification**

It officially informs acceptance, revision, or reject of submitted full paper after the full paper review process.

Status	Action
Acceptance	Go to next Step.
Revision	Re-submit Full Paper within 1 month after Revision Notification.
Reject	Drop everything.

- **Step 4. Payment Registration**

So far it's free of charge in case of the journal promotion paper from the registered ICACT conference paper! But you have to regist it, because you need your Journal Paper Registration ID for submission of the final CRF manuscripts in the next step's process. Once you get your Registration ID, send it to Secretariat@icact.org for further process.

- **Step 5. Camera Ready Form (CRF) Manuscripts Submission**

After you have received the confirmation notice from secretariat of ICACT, and then you are allowed to submit the final CRF manuscripts in PDF file form, the full paper and the Copyright Transfer Agreement. Journal Paper Template, Copyright Form Template, BioAbstract Template,

Journal Submission Guide

All the Out-Standing ICACT conference papers have been invited to this "ICACT Transactions on the Advanced Communications Technology" Journal, and also welcome all the authors whose conference paper has been accepted by the ICACT Technical Program Committee, if you could extend new contents at least 30% more than pure content of your conference paper. Journal paper must be followed to ensure full compliance with the IEEE Journal Template Form attached on this page.

➢ How to submit your Journal paper and check the progress?

Step 1. Submit	Using the Submit button, submit your journal paper through ICACT Website, then you will get new paper ID of your journal, and send your journal Paper ID to the Secretariat@icact.org for the review and editorial processing. Once you got your Journal paper ID, never submit again! Using the Update button, you can change any information of journal paper related or upload new full journal paper.
Step 2. Confirm	Secretariat is supposed to confirm all the necessary conditions of your journal paper to make it ready to review. In case of promotion from the conference paper to Journal paper, send us all the .DOC(or Latex) files of your ICACT conference paper and journal paper to evaluate the difference of the pure contents in between at least 30% more to avoid the self replication violation under scrutiny. The pure content does not include any reference list, acknowledgement, Appendix and author biography information.
Step 3. Review	Upon completing the confirmation, it gets started the review process thru the Editor & Reviewer Guideline. Whenever you visit the Author Homepage, you can check the progress status of your paper there from start to end like this, " Confirm OK! -> Gets started the review process -> ...", in the Review Status column. Please don't miss it!

Volume. 5 Issue. 6

A Novel 5G TDD Cellular System Proposal based on Multipath Division Multiple Access

Wei-Han Hsiao, Chia-Chi Huang

Department of Electrical and Computer Engineering, National Chiao Tung University, Hsinchu, Taiwan, ROC

whsiao.cm97g@g2.nctu.edu.tw, huangcc@faculty.nctu.edu.tw

***Abstract*—Evolving from the 3G and the 4G communication systems, the 5G system demands both high system capacity and high data rate. A novel time division duplexing (TDD) cellular system based on multipath division multiple access (MDMA) with massive antennas in millimeter wave band is proposed in this paper. The system is built on multipath division multiple access which is a method to use massive antennas at BS along with the Rake receiver and the Pre-Rake transmitter to achieve a processing gain for suppressing multiple access interference. The system concept is demonstrated by computer simulations. In addition, the associated transceiver architecture and a TDD time slot structure are presented for practical system concerns. Moreover, it is shown through analysis that the total average data throughput equals 3.8 Gbps and the system can achieve a bandwidth efficiency of 19 bps/Hz/cell on 200 MHz transmission bandwidth.**

***Keyword*—5G communication, cellular system, massive antennas, millimeter wave, TDD**

I. Introduction

Recently, many studies have sprung up in the world [1]-[8] for 5G systems. According to the IMT-2020 released in 2015 [9], stringent system requirements are specified for future 5G systems. On the link level and system level, the next generation 5G mobile radio communication system demands both the high data rate and high system capacity.

Potential technologies for the future 5G system are in the scope of heterogeneous networks, millimeter wave (mmWave) transmission, and massive multiple-input multiple-output (massive MIMO) antennas [8]. The first scheme basically evolves from the Long Term Evolution (LTE) and allows different kinds of cells to function and cooperate in the same geographical area. The second scheme makes use of the unexplored spectrum in the millimeter wave band since it not only avoids frequency spectrum congestion problem below 6 GHz but also provides enough bandwidth for high data rate transmission. Nevertheless, it leads to the inherent problem of much larger propagation loss in much higher frequency bands. The third approach considered employs a large amount of antennas at BS side [10]-[16], usually tens to hundreds of antennas, that offers substantial degrees of freedom for baseband signal processing. Combining millimeter wave transmission with the massive antennas at BS side, this paper presents a multipath division multiple access (MDMA) [17] time division duplexing (TDD) cellular system that is able to provide both the high data rate and high system capacity.

Contributions of this article are briefed in the following. A novel cellular system built upon MDMA for the 5G mobile communication is proposed. In the uplink (UL), MDMA distinguishes its users by exploiting their distinct multipath characteristics through employing RAKE receivers with massive antennas at BS. Similarly, the Pre-RAKE precoding technique with massive antennas is adopted at BS in the downlink (DL). Moreover, every user terminal (UT) is equipped with single antenna that greatly alleviates the signal processing burden. It is shown in Section III that both system capacity and the aggregated data rate can be boosted up to an appreciable extent. Thus, the proposed MDMA TDD cellular system is a promising candidate for future 5G systems.

The paper is organized as follows. Section II gives the radio system architecture, including the transceiver architecture, the associated time slot structure, and a simplified analysis. Section III uses computer simulations as an auxiliary method to illustrate the system concept and provides a simplified analysis to verify the performance of the MDMA system. Finally, the paper completes with conclusions in Section IV.

II. System Architecture

The proposed MDMA cellular system layout is shown in Fig. 1, which operates on the premise of the following assumptions.

1) The system exploits massive antennas operating in the mmWave band, e.g., 30GHz, such that the size of each antenna (e.g., dipole antenna) is very small.
2) The BS antennas are separated by every other 10 wavelengths (at least) to make their received signals nearly uncorrelated [18]. For example, if we arrange 100 antennas in a two-dimensional square grid, then the total

Manuscript received October 24, 2016. This work is a follow-up of the invited journal to an accepted out-standing conference paper of the 18th International Conference on Advanced Communication Technology (ICACT 2016). This research is supported by the Ministry of Science and Technology (MOST) of R.O.C.

W. H. Hsiao is with the Department of Electrical and Computer Engineering, National Chiao Tung University, No.1001, Daxue Rd., East Dist., Hsinchu City 300, Taiwan (R.O.C.) (Corresponding author, Phone: +886-3-5712121 ext. 54579; e-mail: whsiao.cm97g@g2.nctu.edu.tw).

C. C. Huang is with the Department of Electrical and Computer Engineering, National Chiao Tung University, No.1001, Daxue Rd., East Dist., Hsinchu City 300, Taiwan (R.O.C.) (e-mail: huangcc@faculty.nctu.edu.tw).

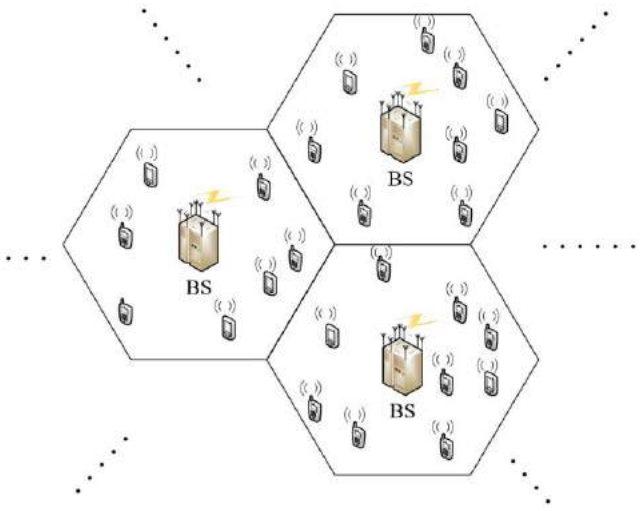

Fig. 1. The proposed MDMA 5G cellular system layout.

area occupied is about 1 m^2, which can be easily deployed in real environments.

3) Channel bandwidth of 200 MHz is assumed in our system. With such wideband transmission, the rich and distinct multipath components of each individual user can be resolved, which helps to distinguish all the users.
4) Time division duplexing (TDD) is adopted here, thus we assume channel reciprocity in uplink and downlink transmissions.
5) UL channel state information (CSI) is known at BS through channel estimation, which can also be used for precoding in DL transmission.
6) Power control is executed in the uplink, i.e., the received power level of each user at BS is nearly equal.
7) A UT is always served by the base station that provides it with the largest received power level.
8) The proposed cellular system is interference limited, i.e., the background noise can be ignored as compared with the interferences.

The equalization of the channel is done in both time and space domains via the Rake receiver and Pre-Rake [19] transmitter in the uplink and downlink, respectively. This leads to a huge signal-to-interference plus noise ratio (SINR) gain for each user when massive antennas are used in the BS. The resultant spatial processing gain is analogous to a CDMA system's processing gain and is effective in suppressing intersymbol interference (ISI), multiple access interference (MAI), and cochannel interference (CCI).

A. Uplink Transceiver Architecture

Fig. 2(a) shows the block diagram of the uplink MDMA transceiver [17]. Consider a multi-user scenario with K single-antenna users and an M-antenna BS in each cell. Assume the binary phase shift keying (BPSK) modulation is used. Then the transmit data bit stream of user k can be written as

$$s_k^{\mathrm{u}}(t) = \sum_n s_k^{\mathrm{u}}(n)\delta(t - nT_b)\ ,\quad k = 1,2,...K\ , \tag{1}$$

where the superscript u, $\delta(\cdot)$, and T_b denote the uplink transmission, the Dirac delta function, and the bit time, respectively. Assume the transmit power $\mathbf{E}\left|s_k^{\mathrm{u}}(t)\right|^2 = 1$ for simplicity, where $\mathbf{E}$ is the expectation operator.

The multipath channel between the kth user and the j-th BS antenna is

$$h_{kj}(t) = \sum_{l=1}^{L} \alpha_{lkj}\delta(t - \tau_{lkj})\ ,\quad k = 1,2,...K.\ j = 1,2,...M\ , \tag{2}$$

where α_{lkj} and τ_{lkj} represent the complex gain and the delay of the l-th path. For normalization, we assume the power gain $\sum_{l=1}^{L}\mathbf{E}\left|\alpha_{lkj}\right|^2 = 1$.

Thus, the received signal at the j-th BS antenna from the k-th user reads

$$\begin{aligned} v_{kj}(t) &= \sum_{l=1}^{L}\sum_n \alpha_{lkj}\, p(t - \tau_{lkj} - nT_b)s_k^{\mathrm{u}}(n) \\ &= s_k^{\mathrm{u}}(t) \otimes p(t) \otimes h_{kj}(t)\ , \end{aligned} \tag{3}$$

where $p(t)$ is the impulse response of the transmit filter with $\int_{-\infty}^{\infty} p^2(t)\,dt = 1$ and $\otimes$ denotes the linear convolution operator.

Hence, the output of the k-th user's Rake receiver at the j-th BS antenna equals to

$$\begin{aligned} u_{kj}(t) &= \left(v_{kj}(t) + \sum_{\substack{q=1 \\ q\neq k}}^{K} v_{qj}(t) + \mathrm{CCI} + n_j(t) \right) \\ &\quad \otimes \sum_{l'=1}^{L} \alpha_{l'kj}^{*}\, p^{*}(-t - \tau_{l'kj}) \\ &= \left(\begin{array}{l} s_k^{\mathrm{u}}(t) \otimes p(t) \otimes h_{kj}(t) + \sum\limits_{\substack{q=1 \\ q\neq k}}^{K} s_q^{\mathrm{u}}(t) \otimes p(t) \otimes h_{qj}(t) \\ + \mathrm{CCI} + n_j(t) \end{array} \right) \\ &\quad \otimes p^{*}(-t) \otimes h_{kj}^{*}(-t)\ , \end{aligned} \tag{4}$$

where $n_j(t)$ is the additive white Gaussian noise at the j-th BS antenna and the cochannel interference (CCI) comes from other cells. Note that the Rake receiver here is represented by $p^{*}(-t) \otimes h_{kj}^{*}(-t)$, where $*$ denotes the complex conjugation.

Finally, the BS detects the n-th data bit of user k according to the decision metric $\sum_{j=1}^{M} u_{kj}(t)$ at $t = nT_b$.

B. Downlink Transceiver Architecture

Fig. 2(b) shows the corresponding block diagram of the downlink transceiver. The data bit stream of each user is precoded by the Pre-Rake transmitter for each BS antenna. Meanwhile, the required CSI is obtained through uplink channel estimation and it is used for Pre-Rake precoding. It is worth noting that the Pre-Rake precoding moves the equalization effort to the BS transmitter that helps to reduce the complexity of the UT receiver.

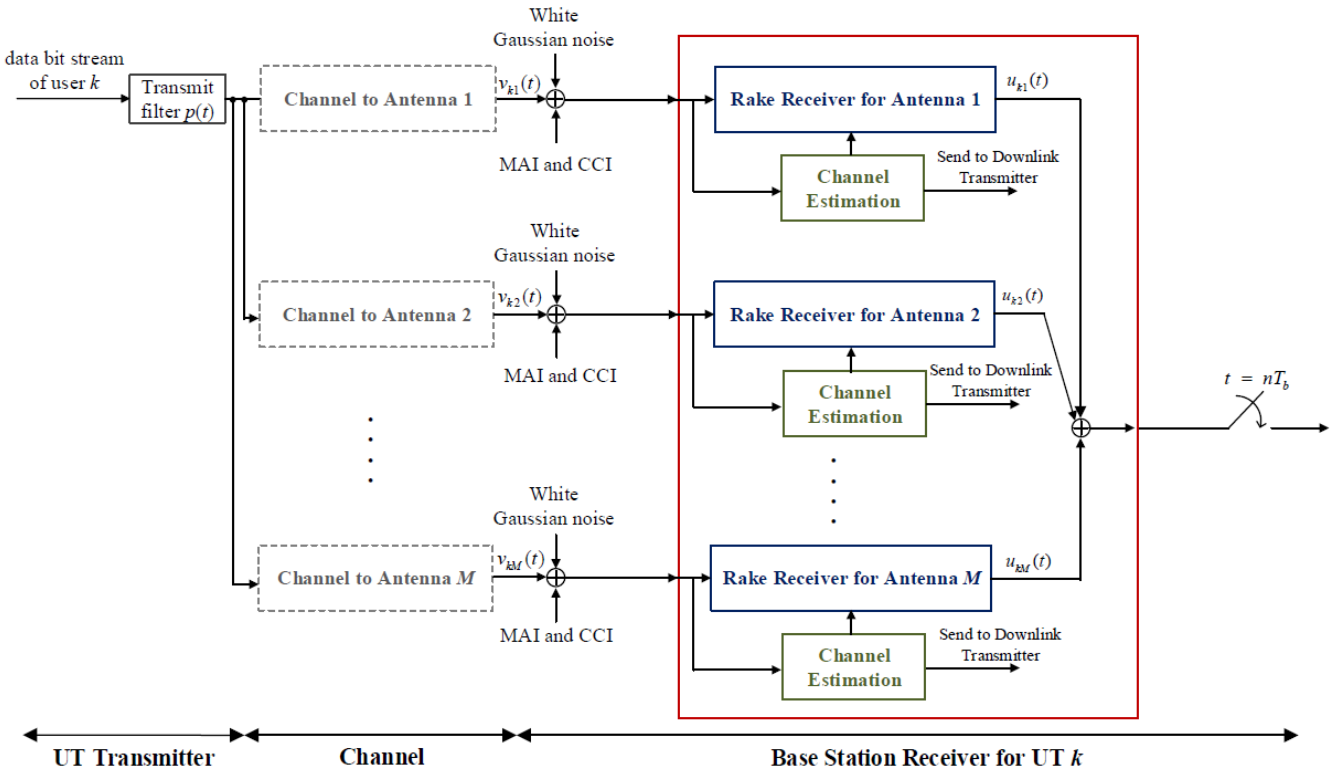

(a)

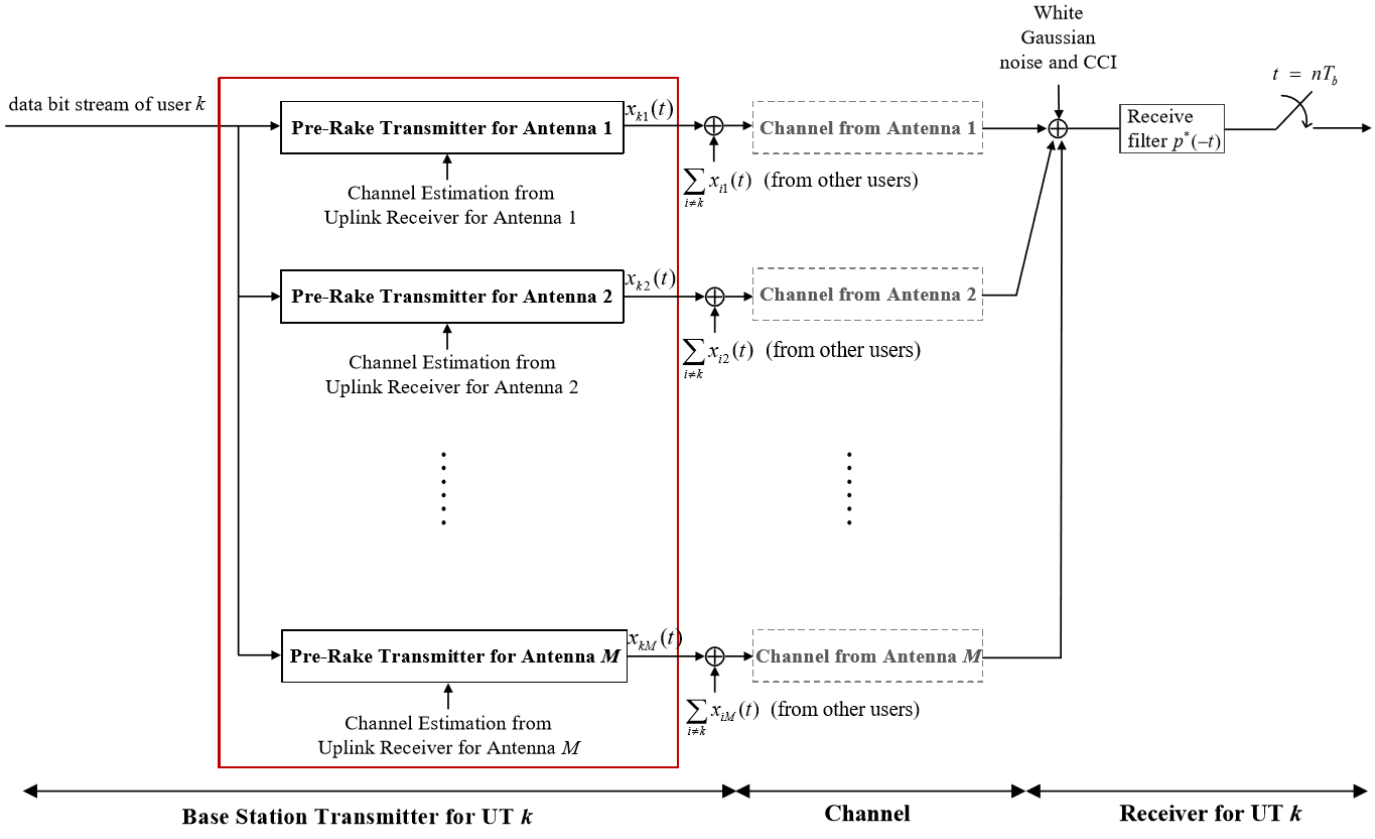

(b)

Fig. 2. MDMA transceiver architecture for (a) uplink and (b) downlink.

The output of the user k's Pre-Rake transmitter for antenna j is

$$x_{kj}(t) = s_k^{\mathrm{d}}(t) \otimes p^*(-t) \otimes h_{kj}^*(-t) = \sum_{l=1}^{L} \sum_{n} \alpha_{lkj}^* p^*(t + \tau_{lkj} - nT_b) s_k^{\mathrm{d}}(n) , \quad (5)$$

where the superscript d denotes the downlink transmission.

Thus, the transmitted signal at the j-th antenna is $\sum_{k=1}^{K} x_{kj}(t)$, i.e., the sum over all the users' Pre-Rake transmitter outputs for the j-th BS antenna.

In the user terminal, the data is detected by sampling the received signal at the correct sampling time and making decisions accordingly.

C. Simplified Analysis

An analysis of the single cell scenario is considered here from link level point of view while the multi-cell scenario is discussed in Section III from system capacity point of view.

Since the Rake reception and the Pre-Rake transmission provide the same signal-to noise ratio (SNR) as proved in [19] for single BS antenna case, we only show here the uplink SIR performance of the system with massive antennas at BS.

Assume user k represents the desired user. Insert (3) into (4) and neglect MAI, CCI and noise terms for now, we get

$$u_{kj}(t) = \int_{-\infty}^{\infty} \left(\sum_{l=1}^{L} \sum_{m} \alpha_{lkj} p(\lambda - \tau_{lkj} - mT_b) s_k(m) \right) \times \left(\sum_{l'=1}^{L} \alpha_{l'kj}^* p^*(-t + \lambda - \tau_{l'kj}) \right) d\lambda . \quad (6)$$

Here, we use a bandlimited filter $p(t) = \frac{1}{\sqrt{T_b}} \mathrm{sinc}\left(\frac{t}{T_b}\right)$ since it satisfies not only $\int_{-\infty}^{\infty} p^2(t)\, dt = 1$ but also the Nyquist criterion, i.e., $p_{eff}(iT_b) = \delta[i]$, $i \in \mathbb{Z}$, where $\delta[n]$ is the Kronecker delta function and $p_{eff}(t) \equiv p(t) \otimes p^*(-t)$.

Thus, sampling (6) at $t = nT_b$ results in

$$\begin{aligned} u_{kj}(nT_b) &= \int_{-\infty}^{\infty} \left(\sum_{l=1}^{L} \sum_{m} \alpha_{lkj} p(\lambda - \tau_{lkj} - mT_b) s_k^{\mathrm{u}}(m) \right) \times \left(\sum_{l'=1}^{L} \alpha_{l'kj}^* p^*(-nT_b + \lambda - \tau_{l'kj}) \right) d\lambda \\ &= \int_{-\infty}^{\infty} \left(\sum_{l=1}^{L} |\alpha_{lkj}|^2 p^2(\lambda - \tau_{lkj} - nT_b) s_k^{\mathrm{u}}(n) \right) d\lambda + \mathrm{ISI} \\ &= s_k^{\mathrm{u}}(n) + \mathrm{ISI} . \end{aligned} \quad (7)$$

The last equality holds due to wideband transmission, say 200 MHz in our system. That is, $\sum_{l=1}^{L} |\alpha_{lkj}|^2 \cong \sum_{l=1}^{L} \mathbf{E}|\alpha_{lkj}|^2 = 1$ for large L. Combine *coherently* all the Rake receiver's outputs and sample at time nT_b for user k, one can get the desired signal as $Ms_k^{\mathrm{u}}(n)$, i.e., the desired signal power becomes M^2 times of that in the single-antenna case.

Since the interference mainly comes from other users in the same cell, i.e., MAI can be modeled as

$$z_k(t) = \sum_{j=1}^{M} \sum_{q \neq k} s_q^{\mathrm{u}}(t) \otimes p(t) \otimes h_{qj}(t) \otimes h_{kj}^*(-t) \otimes p^*(-t) = \sum_{j=1}^{M} \sum_{q \neq k} s_q^{\mathrm{u}}(t) \otimes \left[p(t) \otimes p^*(-t) \right] \otimes h_{qj}(t) \otimes h_{kj}^*(-t) = \sum_{j=1}^{M} \sum_{q \neq k} s_q^{\mathrm{u}}(t) \otimes p_{eff}(t) \otimes h_{qj}(t) \otimes h_{kj}^*(-t) . \quad (8)$$

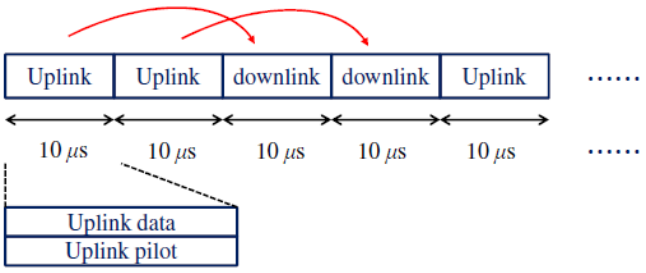

Fig. 3. The proposed time slot structure

Due to the channel's randomness and normalization among all users, the interference power from MAI in (8) can be calculated as $M(K-1)$ according to [23, p.5]. Note that we assume the channel has unit power gain. In fact, the result is a direct consequence of the *noncoherent* addition of the interference terms over all receive BS antennas.

We can easily calculate the equivalent E_b/I_0 of each user and the result is approximately equal to M/K when M is large. Since massive antennas are used at BS, the equivalent E_b/I_0 could be boosted up to a required amount. In other words, the end-to-end equivalent channel of each user gradually approaches an ideal channel, an impulse-like channel, when M is large. Thus, M is the processing gain which can be offered by the MDMA cellular system. Similarly, an equal amount of processing gain can be achieved for each DL user through Pre-RAKE precoding.

D. Time Slot Structure

Since the channel coherence time at a carrier frequency of 1 GHz and a vehicle speed of 100 km/hr is roughly 600 μs[1] [20], the corresponding coherence time at 30 GHz is about 20 μs, because it is inversely proportional to the carrier frequency. Therefore, the system we considered needs to estimate the channel with a time period of 20 μs. Fig. 3 shows the time slot structure of the TDD cellular system. A time slot (TS) duration of 10μs amounts to 2000 bits for both UL and DL. Two DL time slots directly follow two UL time slots. Together with the data signal, the UL time slots also transmit a pilot signal with the same power level as the data signal for the purpose of channel estimation. Furthermore, a 10 μs processing time is reserved such that the channel estimation result in the first UL TS can be used for the first DL TS while the second UL TS channel estimation result is used for the second DL TS, as the red arrows point out in Fig. 3. Although this pilot-added approach inevitably causes extra interference for UL data detection, advanced signal processing techniques such as iterative cancellation can be applied to reduce the interference effect. The relevant channel estimation and interference cancellation techniques, out of the scope of this article, are treated in another paper.

[1] Recall that the packet duration in GSM is 577 μs, in this time period the channel can be regarded as quasi-static at a vehicle speed of 100 km/hr in 1 GHz band [20].

III. Computer simulation and system capacity evaluation

In the computer simulations which are used to illustrate the MDMA cellular system concept, we modify the S-V channel model according to the spatial parameters given in [21]. First, we generate the number of clusters by the Poisson distribution. Then, the arrival time of the different clusters is set to be uniformly distributed within the maximum delay spread, e.g., 404.1 ns [22]. Second, we calculate the power of each cluster using the model of [21]. Third, we generate the inter-arrival time of each ray within individual cluster according to the exponential distribution. Finally, we calculate the power of each ray. In addition, the time resolution of multipath in our 5G system is equal to 5 ns (due to 200 MHz channel bandwidth), which is the same as the time resolution in the original S-V model. Thus, the path delay is quantized to the nearest integer multiple of 5 ns. Note that a ray will be dropped when its power is less than a predefined threshold, e.g., 10 dB below the strongest path. A realization of the channel impulse response is plotted in Fig. 4.

Fig. 5 shows an effective end-to-end channel of a desired user in a single cell which serves 25 users simultaneously. The effective end-to-end channel of user k is defined here as the discrete-time version of $\sum_{j=1}^{M}\sum_{q=1}^{K} h_{qj}(t) \otimes h_{kj}^{*}(-t)$. It is apparent that as the number of BS antennas increases, the interferences get more suppressed relative to the desired signal, which agrees with the simplified analysis in Section II C when M grows large. That is, the interferences including MAI and ISI can be suppressed with a large number of BS antennas. Moreover, the power of the desired signal is nearly M^2 times as expected.

Fig. 6 plots the cumulative distribution of the uplink receive SIR with 100 BS antennas and different number of users in a *multi-cell* scenario. In the simulations, the cellular system is constructed with 127 hexagonal cells (each with a radius of 250 m) which include 6 tiers of cochannel cells. For simplicity, assume uplink channel is known at BS in advance. Some observations can be made here. First, it can be observed that the mean of receive SIR is proportional to M / K which matches the simplified analysis result in the previous section. Similarly, the SIR distribution gets improved as the ratio of M / K increases. On one hand, the mean of the receive SIR is less than M / K by a factor of $2 / 3$ (-1.7 dB) which is caused by all the other cell interference. On the other hand, variations around the mean of the receive SIR diminish as the number of users increases due to the law of large numbers. That is, the receive SIR converges to its mean as more users are served in the system. Fig. 7 plots the cumulative distribution of the downlink receive SIR. Again, it reveals that the mean of receive SIR is proportional to M / K as in the downlink. However, the receive SIR distribution is worse than the uplink case since higher tail probability can be observed. This is because there is no power control in the downlink, which causes more serious cochannel interference problems.

Here, we define $f_{99\%}$ to be the other-cell relative interference factor for the worst 1% in the SIR cumulative distribution functions, i.e., the probability that the SIR value exceeds a predefined SIR threshold is greater than 0.99. In [24], $f_{99\%}$ is found to be 0.7 in the uplink with power control, while it is relatively larger and is about 3.6 in the downlink without power control. By examining the initial portion of Fig. 6 and Fig. 7 closely, we found these values ($f_{99\%} = 0.7$ or 3.6) are consistent with our simulation results with hexagonal cell layout, such that they are applied here.

Toward the MDMA TDD cellular system, a simple evaluation of its system capacity is given here. Recall that the system considered operates in the carrier frequency of 30 GHz with a channel bandwidth of 200 MHz, and has a frequency reuse factor of one. Also note that K and M are the number of users in a cell and the number of BS antennas respectively. Assume BPSK modulation and ideal power control in the uplink. In the worst case, the system is in full loading, i.e., K users are transmitting concurrently. In this situation, the SIR at each user's demodulator output is thus

$$\frac{E_b}{I_0} \cong \frac{S}{I} = \frac{M^2}{M(K-1)} \times \frac{1}{1+f_{99\%}} = \frac{M}{K-1} \times \frac{1}{1+f_{99\%}}, \tag{9}$$

where E_b and I_0 represent the received energy per bit and the interference power spectrum density. S and I are respectively the average signal power and interference power. $\frac{M^2}{M(K-1)}$ comes from the fact that the desired signal of each BS antenna adds coherently while the interference sums up noncoherently.

Rearranging (9) leads to

$$K \cong \frac{M}{E_b/I_0} \times \frac{1}{1+f_{99\%}}, \tag{10}$$

which gives an elegant formula to calculate the number of users the BS can serve under the required E_b / I_0 at each user's demodulator output.

We consider first data transmission in the uplink time slots as described in Section II with half power allotted to data and pilots. Assume a minimum E_b / I_0 of 6 dB for data detection that provides the acceptable performance [23, pp.8], 300 BS antennas can serve 22 full loaded users in every cell simultaneously, since $\frac{300}{4} \times \frac{1}{1+0.7} \times \frac{1}{2} \cong 22$, where the last one-half factor counts for the reduction in SIR due to uplink pilots. Now we consider transmission in the downlink time slots. Since there are no pilots used in the downlink, the total number of simultaneous users which can be served turns out to be $\frac{300}{4} \times \frac{1}{1+3.6} \cong 16$. In a real system, the number of simultaneous users can be greatly increased if they are not full loaded.

Since each user in the cell shares the whole 200 MHz bandwidth, the proposed TDD cellular system can at least provide a total average data throughput of 200 Mbps $\times$ $(22+16)\times\frac{1}{2} = 3.8$ Gbps. Thus, the system achieves a bandwidth efficiency of 19 bps/Hz/cell.

Note that the system capacity can be further enhanced if multi-user detection techniques (e.g., successive interference cancellation or parallel interference cancellation) are used to eliminate intra-cell interference. The system capacity can be increased since the factor $1 / (1+f_{99\%})$ in (10) could be replaced by $1 / f_{99\%}$ if the intra-cell interference can be totally cancelled.

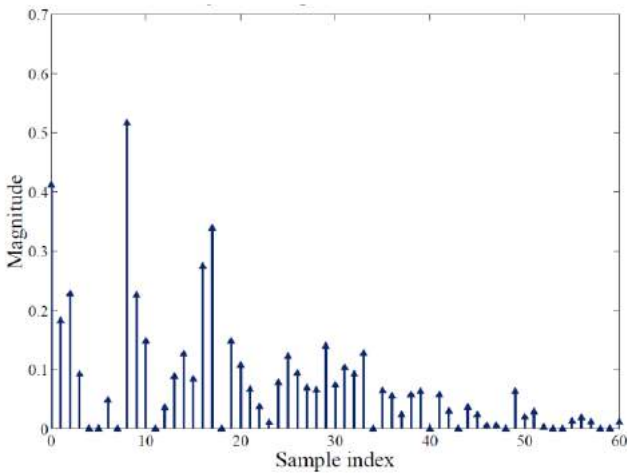

Fig. 4. A realization of the channel amplitude response.

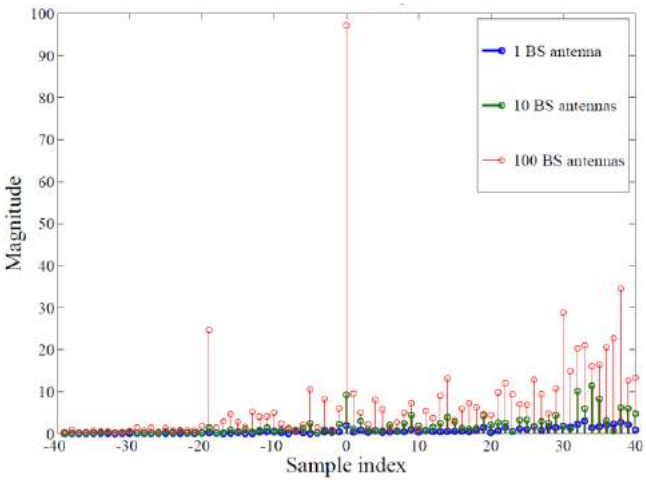

Fig. 5. An effective end-to-end channel of a desired user in a full loading cell with 25 active users.

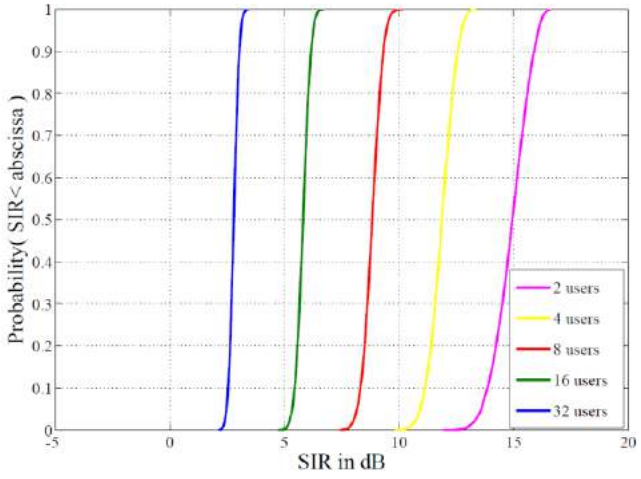

Fig. 6. The cumulative distribution of the uplink receive SIR with 100 BS antennas and different number of active users in a multi-cell scenario.

IV. Conclusion

The next generation (5G) cellular communication system demands both high system capacity and high data rate. A novel cellular system architecture built upon MDMA is proposed for the future 5G cellular mobile communication. MDMA is a multiple access method to use massive antennas at BS together with the Rake receiver and the Pre-Rake

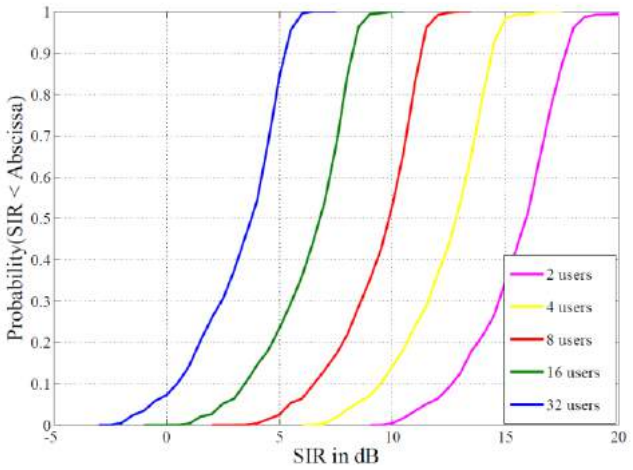

Fig. 7. The cumulative distribution of the downlink receive SIR with 100 BS antennas and different number of active users in a multi-cell scenario.

transmitter to achieve a processing gain to suppress multiple access interference in a TDD cellular mobile radio system. The transceiver architecture and the TDD time slot structure are described in the article. On the other hand, the user terminal is kept simple because only single antenna is used for every user. From simulations and simple analysis, it is shown that both system capacity and aggregated data throughput can be boosted up to a considerable level for a cellular system with a frequency reuse factor of one. The system can serve on average 19 ($=(22+16)\times 0.5$) users in each cell with the total average data throughput of 3.8 Gbps on 200 MHz transmission bandwidth which achieves a bandwidth efficiency of 19 bps/Hz/cell. In brief, the proposed MDMA TDD cellular system can serve as a candidate system architecture for future 5G wireless communication.

References

[1] METIS website. (2015) [Online]. Available: https://www.metis2020.com

[2] European Commission. (2013). 5GNOW-5th Generation Non-Orthogonal Waveforms for Asynchronous Signaling. [Online]. Available: http://cordis.europa.eu/fp7/ict/future-networks/documents/call8-projects/5gnowfactsheet.pdf

[3] Alcatel-Lucent. (2011). LTE and beyond, [Online]. Available: http://web.dit.upm.es/~doct/SI/2011-2012

[4] NTT DOCOMO, "Future Radio Access for 5G", white paper, Jul. 2014

[5] W. Roh. (2013). Performances and Feasibility of mmWave Beamforming Prototype for 5G Cellular Communications. Presented at IEEE ICC. [Online]. Available: http://www.faculty.poly.edu/~tsr

[6] G. Wunder *et al*., "5GNOW: Challenging the LTE Design Paradigms of Orthogonality and Synchronicity," *2013 IEEE 77th Vehicular Technology Conference (VTC)*, Jun. 2013.

[7] A. Osseiran *et al.*, "The foundation of the mobile and wireless communications system for 2020 and beyond: challenges, enablers and technology solutions," *2013 IEEE 77th Vehicular Technology Conference (VTC)*, Jun. 2013.

[8] J. G. Andrews *et al.*, "What will 5G be?," *IEEE Journal on Sel. Areas in Communications*, vol. 32, no. 6, pp. 1065−1082, Jun. 2014.

[9] ITU website. (2015) [Online]. Available: http://www.itu.int/en

[10] T. L. Marzetta, "Noncooperative cellular wireless with unlimited numbers of base station antennas," *IEEE Trans. on Wireless Communications*, vol. 9, no. 11, pp. 3590−3600, Nov. 2010.

[11] A. Pitarokoilis, S. K. Mohammed, and E.G. Larsson, "On the optimality of single-carrier transmission in large-scale antenna systems," *IEEE Wireless Communications Letters*, vol. 1, no. 4, pp. 276−279, Aug. 2012.

[12] J. Hoydis, S. ten Brink, and M. Debbah, "Comparison of linear

precoding schemes for downlink massive MIMO," *2012 IEEE International Conference on Communications (ICC)*, pp. 2135–2139, Jun. 2012.
[13] F. Rusek *et al*., "Scaling up MIMO: opportunities and challenges with very large arrays," *IEEE Signal Processing Magazine*, vol. 30, no. 1, pp. 40–60, Jan. 2013.
[14] J. Zhang *et al*., "On capacity of large-scale MIMO multiple access channels with distributed sets of correlated antennas," *IEEE Journal on Sel. Areas in Communications*, vol. 31, no. 2, pp. 133–148, Feb. 2013.
[15] J. Hoydis, S. ten Brink, and M. Debbah, "Massive MIMO in the UL/DL of cellular networks: how many antennas do we need?," *IEEE Journal on Sel. Areas in Communications*, vol. 31, no. 2, pp. 160–171, Feb. 2013.
[16] E. Larsson *et al*., "Massive MIMO for next generation wireless systems," *IEEE Communications Magazine*, vol. 52, no. 2, pp. 186–195, Feb. 2014.
[17] W. H. Hsiao and C. C. Huang, "Multipath division multiple access for 5G cellular system based on massive antennas in millimeter wave band," the *18th Intl. Conf. on Advanced Communications Technology (ICACT)*, pp.741–746, Jan. 2016.
[18] C. Y. Lee, "Mobile radio performance for a two-branch equal-gain combining receiver with correlated signals at the land site," *IEEE Trans. on Vehicular Technology*, vol. 27, no. 4, pp. 239–243, Nov. 1978.
[19] R. Esmailzadeh and M. Nakagawa, "Pre-RAKE diversity combination for direct sequence spread spectrum mobile communications systems," *IEICE Trans. Communications.*, vol. E76-B, no. 8, pp. 1008–1014, Aug. 1993.
[20] T. S. Rappaport, *Wireless Communications: Principles and Practice*, 2nd ed., Prentice Hall, 2002.
[21] M. R. Akdeniz, Y. Liu, S. Sun, S. Rangan, T. S. Rappaport, and E. Erkip, "Millimeter wave channel modeling and cellular capacity evaluation," *IEEE Journal on Sel. Areas in Communications*, Sep. 2014.
[22] S. Sun and T. S. Rappaport, "Multi-beam antenna combining for 28 GHz cellular link improvement in urban environments," in *Proc. IEEE Globecom*, Dec. 2013.
[23] A. J. Viterbi, *CDMA: Principles of Spread Spectrum Communication*, Prentice Hall, 1995.
[24] C. C. Huang, "Computer simulation of a direct sequence spread spectrum cellular radio architecture," *IEEE Trans. on Vehicular Technology*, vol. 41, no. 4, pp. 544–550, Nov. 1992.

Wei-Han Hsiao was born in Taiwan, R.O.C. He received the B.S. degree in electrical and control engineering from National Chiao Tung University (NCTU), Hsinchu, Taiwan, in 2008. He is currently pursuing the Ph.D. degree in communications engineering since 2010 in NCTU. His current research interests are on transceiver design and analysis for next generation mobile communication systems**.**

Chia-Chi Huang was born in Taiwan, R.O.C. He received the B.S. degree in electrical engineering from National Taiwan University in 1977 and the M.S. and Ph.D. degrees in electrical engineering from the University of California, Berkeley, in 1980 and 1984, respectively.

From 1984 to 1988, he was an RF and communication system engineer with the Corporate Research and Development Center, General Electric Company, Schenectady, NY, where he worked on mobile radio communication system design. From 1989 to 1992, he was with the IBM T.J. Watson Research Center, Yorktown Heights, NY, as a Research Staff Member, working on indoor radio communication system design. Since 1992, he has been with National Chiao Tung University, Hsinchu, Taiwan, and currently as Professor in the Department of Electrical and Computer Engineering. His research areas are in mobile radio, wireless communication, and cellular systems.

Coexistence of Korea's DVB-T2 and Japan's ITS using 700MHz frequency band

Ho-Kyung Son, Young-Jun Jung

Radio Technology Research Department, Electronic Telecommunication Research Institute, Daejon, Korea

hgson@etri.re.kr, yjchong@etri.re.kr

***Abstract*—In this paper, we analyze the effects of interference between Korea's ultra-high definition TV broadcasting system and Japan's intelligent transport system using the 700 MHz frequency band when considering a practical deployment of both systems. We performed Minimum Coupling Loss (MCL) method to evaluate how much interference from the Korean UHDTV system is imposed on the Japan ITS system. We also employ the Advanced Propagation Model (APM) and ITU-R P. 452-15 model to calculate the propagation loss occurring in ducts. Our study can be applied to the deployment planning for each system with an interference impact acceptable to both parties.**

***Keyword*—DVB-T2, ITS, Interference, Ducting**

I. INTRODUCTION

Many countries converted their analog TV systems into digital TV (DTV). The South Korean government also allocated CH 14 through CH 51 (470-698 MHz) for DTV use [1] and recently determined to allocate additionally 30MHz (698-710 MHz and 753-771 MHz) for ultra-high definition TV (UHDTV) use [2]. Several broadcasters did test broadcasting with Digital Video Broadcasting-Terrestrial version 2 (DVB-T2) standard. But recently the Korean government picked the Advanced Television Systems Committee (ATSC) 3.0 standard for ultra-high-definition (UHD) television broadcasting set to launch next year [3].

In Japan, digital terrestrial TV broad-casting service is available at 460-710 MHz on the UHF band using the ISDB-T standard and a 9 MHz channel width in the 755.5-764.5 MHz radio frequency band will be used for Intelligent Transport System (ITS). It is the realization of safe driving support systems to reduce the number of traffic accidents. The 700 MHz frequency band is known for its good propagation characteristics in non-line-of-sight conditions such as behind buildings or large vehicles [4]. The 755.5-764.5 MHz frequency band partially overlaps with Korean UHDTV frequency band.

Although Korean UHDTV system and Japan ITS system are located with a sufficient separate distance, the potential interference would be produced. A few years ago, radio interference began to occur in the Trunked Radio Service (TRS) frequency band in the southern coastal area of Korea [5] and similar interference has also been observed in the mobile communication frequency band [6]. Monitoring such radio interference found that its main source was the ducting of radio signals produced in the coast of Japan.

The ducting of an RF signal is caused by an atmospheric anomaly known as temperature inversion. A layer of ice cold or very hot air traps the RF signal and guides it to a farther distance than expected through an anomalously formed duct. These ducts can extend to hundreds or even thousands of miles. Once trapped, the ducted signal may cause interference to distant wireless systems [7]. As the height and duration of the duct layer are not constant, it is difficult to predict the effects of this type of interference. To allow better radio communication services, we need to be able to predict the effects of interference and study a method of coexistence between the two countries.

In this paper, we analyze the effects of interference between UHDTV services in Korea and ITS service in Japan at the 700 MHz frequency band. We focus particularly on an interference scenario of Korea's UHDTV to Japan's ITS, as this type of interference is more serious than the other interference scenario. Korean UHDTV is assumed in DVB-T2 system and the Minimum Coupling Loss (MCL) method is used for the interference analysis between fixed stations. We also employ the Advanced Propagation Model (APM) and ITU-R P. 452-15 model to calculate the propagation loss occurring in ducts. To protect against interference between Korean and Japanese radio signals, the required additional attenuation loss according to the UHDTV's antenna tilt degree is also calculated.

This paper is organized as follows. In section II, interference scenarios and the interference analysis method are described. In addition, the propagation model used are presented. The simulation parameters and results are presented in section III. Finally, some concluding remarks regarding our proposal are provided in section IV.

Manuscript received October 20, 2016. This work was supported by the ICT R&D program of MSIP/IITP [B0101-15-222, Development of core technologies to improve spectral efficiency for mobile big-bang] and a follow-up of the invited journal to the conference paper of the 18th International Conference on Advanced Communication Technology (ICACT2016).

Ho-Kyung Son is with radio technology research department, Electronics and Telecommunications Research Institute, Daejeon, Republic of Korea (Corresponding author, phone: +82-42-860-5981, fax:+82-42-860-5199, email:hgson@etri.re.kr)

Young-Jun Jong is with radio technology research department, Electronics and Telecommunications Research Institute, Daejeon, Republic of Korea (email:hjhong@etri.re.kr)

II. INTERFERENCE SCENARIO AND METHODOLOGY

A. Interference scenario

Fig. 1 shows a scenario for interference analysis from Korea's DVB-T2 system to Japan's ITS system. We assumed that Korea's DVB-T2 site transmits signals using the 759-765 MHz frequency band and Japan ITS system has a 9 MHz channel bandwidth using 755.5-764.5 MHz frequency band. The distance between Korea and Japan ranges from about 240 to 300 km, we assumed the separate distance between two systems is 240 km.

Japan ITS systems are supposed to consist of two types of systems: vehicle-to-vehicle communication systems that support safe driving by inter-vehicular radio communications at intersections with poor visibility, and roadside-to-vehicle communication systems that support safe driving by sending information from roadside units of traffic infrastructure to vehicles through radio communications [4]. We considered only roadside-to-vehicle communication systems that vehicle transmit the signal to roadside units. We evaluated whether the received interference power at the antenna of Japan's ITS receiver satisfies the maximum allowable interference power.

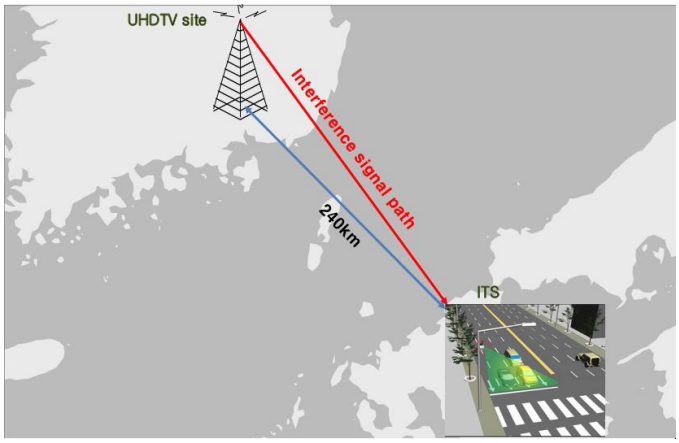

Fig. 1. Interference scenario between Korea's DVB-T2 and Japan's ITS

B. Methodology for an interference analysis

The possibility of frequency spectrum sharing depends on whether the received signal-to-interference plus noise ratio at the antenna of victim receiver satisfies the minimum signal-to-interference plus noise needed to process (vice just detect) a signal.

$$P_S - (P_N + P_I) \geq SINR_{\min} \quad (1)$$

where P_S is the received wanted signal power from vehicle's transmitting signal, P_N is the thermal noise power of the receiver and P_I is the received interfered signal power from Korean DVB-T2 transmitting signal.

The received interfered signal power from Korean DVB-T2 transmitting signal is expressed by [8]

$$P_I = P_t + G_t + G_r - PL(d) \quad (2)$$

where P_t is the transmit power of the interfering system in the reference bandwidth in dBm, G_t is the gain of the interferer antenna in the direction of the receiver in dBi, G_r is the gain of the victim receiver antenna in the direction of the interferer in dBi, $PL(d)$ is a basic transmission loss for separation distance d between the interferer and receiver in dB.

The receiver thermal noise power is given by

$$P_N = 10\log_{10}(kTB) + NF \quad (3)$$

where k is Boltzmann's constant (W/K/Hz), T is the ambient temperature (K), B is the channel bandwidth (Hz), and NF is the receiver noise figure (dB). For $k = 1.3804 \times 10^{-23}$, T=290 and NF=6dB, we have $P_N = -108\,dBm/MHz$.

In an interference-limited environment, equation (1) can be approximated as follow

$$P_N + P_I \approx P_I \quad (4)$$

The tolerable interference signal power can be determined using the following equation

$$P_{I,target} \leq P_S - SINR_{\min} \quad (5)$$

The required additional attenuation loss (L_a), in dB, of the interfering system on the victim system can be determined using the following equation [8]:

$$L_a = P_I - P_{I,target} \quad (6)$$

$P_{I,Target}$ is the tolerable, or target, interference power at the receiver.

C. Propagation model for path loss calculation

The basic transmission loss is the most important factor to predict the interference level and determine the additional required attenuation loss. For a calculation of this basic transmission loss occurring in a duct, we used ITU-R P.452-15 [9] and hybrid propagation model called an Advanced Propagation Model (APM).

ITU-R P.452-15 is a prediction method for the evaluation of interference between stations on the surface of the Earth at frequencies from about 0.1 GHz to 50 GHz, accounting for both clear-air and hydrometeor scattering interference mechanisms. The models within Recommendation ITU-R P.452 are designed to calculate propagation losses not exceeded for time percentages over the range $0.001 \leq p \leq 50\%$. This assumption does not imply the maximum loss will be at $p = 50\%$. The method includes a complementary set of propagation models which ensure that the predictions embrace all the significant interference propagation mechanisms that can arise. Methods for analyzing the radio-meteorological and topographical features of the path are provided so that predictions can be

prepared for any practical interference path falling within the scope of the procedure up to a distance limit of 10000 km [9].

APM is much faster than split-step parabolic equation (PE) method, yet it requires far less memory and can be used in wider applications. APM considers four regions shown in Fig. 2. At ranges less than 2.5km and for all elevation angles above 5°, APM uses a flat earth (FE) model region. For beyond the FE region, where the grazing angles of the reflected rays from the transmitter are above a small limiting value, the ray optics (RO) model is used. The PE model is used for ranges beyond the RO region, but only for altitudes below a maximum PE altitude as determined by the maximum allowed 1024-point Fast-Fourier transform (FFT). For ranges beyond the RO region and heights above the PE region, an extended optics (XO) method is allowed, which can operate at the maximum PE altitude [10].

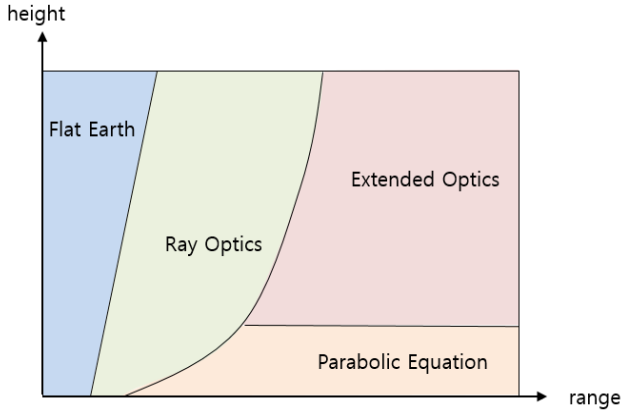

Fig. 2. Advanced Propagation Model(APM)

III. Simulation Results

A. Simulation parameter

We considered a scenario of the interference between Korea's DVB-T2 and Japan's ITS, where DVB-T2 and ITS are deployed at the shores of Korea and Japan. We simulated only the interference effect from Korea's DVB-T2 station to Japan's ITS road station. Table I and II present the operational system parameters for the DVB-T2 and ITS systems used for simulation, respectively. We consider the DVB-T2's channel bandwidth to be 6 MHz and the transmitting power to be 5 kW. Hwang-Ryeong Mountain was chosen as Korean DVB-T2 site, which located near Japan. The vertical pattern of the DVB-T2 antenna [11] was shown in Fig. 3. We consider the channel bandwidth of ITS system to be 9 MHz and the vehicles transmitting power to be 200 mW. We also assumed 7m as the Road-side antenna height and 13dB minimum SNR as the protection ratio. Also we consider the Road-side noise figure is 6dB. A free space propagation model is used to calculate the path loss between ITS's vehicle and ITS's roadside.

TABLE I
DVB-T2 SYSTEM PARAMETERS FOR SIMULATION

Parameter		Value
Center frequency		762MHz
Channel bandwidth		6MHz
Transmitting power		67dBm
Antenna gain		10dBi
Antenna height		450m
Distance		240km
Modified refractivity		WMO data
tilting		0°~9°
Location		35° 15′ 80″
		129° 08′ 22″
Antenna pattern	horizontal	omni
	vertical	ITU-R F. 1336

TABLE II
ITS SYSTEM PARAMETERS FOR SIMULATION

Parameter	Value
Center frequency	760MHz
Channel bandwidth	9MHz
Vehicles radiated power	20dBm
Road-side antenna height	7m
Road-side antenna gain	13dBi
Road-side noise figure	6dB
Minimum SNR	13dB
Vehicle antenna height	3m
Vehicle antenna gain	0dBi

An ITU-R P.452-15 propagation model and APM are used to calculate the path loss between Korea's DVB-T2 and Japan's ITS and Table III shows the path loss using the P.452-15 model. Table IV shows the modified refractivity index of Pohang provided by the WMO station. The values represent a surface-based duct and elevated ducts in June.

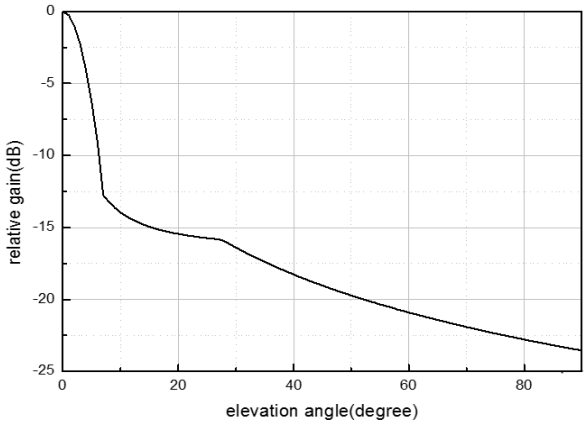

Fig. 3. DVB-T2's antenna vertical pattern

TABLE III
PATH LOSS USING ITU-R P.452-15

Time rate(%)	Path loss(dB)
1	144.2dB
10	172.8dB
50	179.6dB

TABLE IV
MODIFIED REFRACTIVITY-WMO DATA

Height(m)	Modified refractivity
0	337
16	339
47	343
72	334
1933	559
2055	551
3054	661

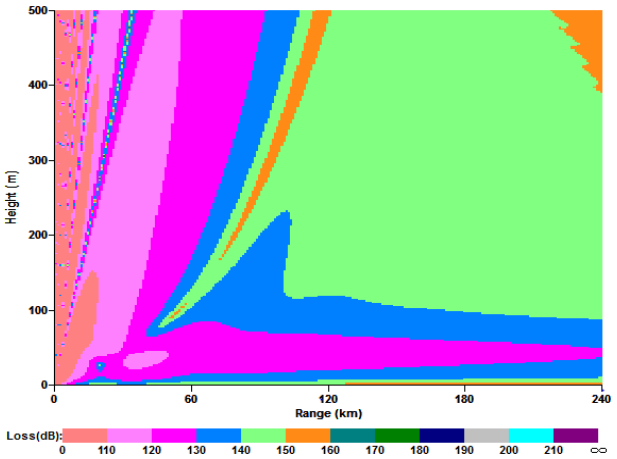

Fig. 4. Path loss between Korean DVB-T2 and Japan ITS using APM

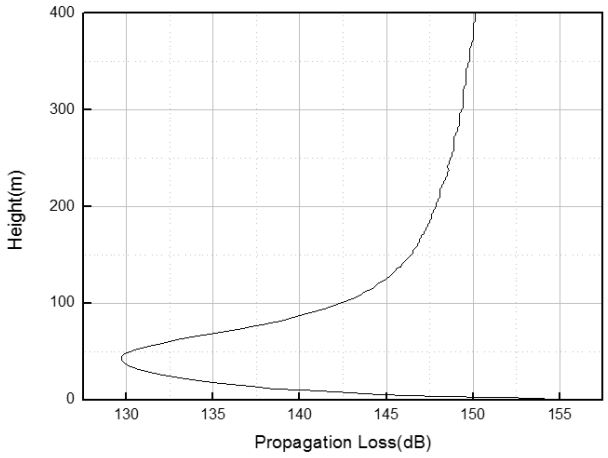

Fig. 5. Path loss versus receiving antenna height

B. *Simulation result*

The propagation loss using APM for variation of the distance between Korea's DVB-T2 and Japan's ITS is shown in Fig.4. The propagation loss appears to increase as the distance is increased and the propagation loss by ducting may be smaller than the free space loss.

Fig. 5 shows the propagation loss for variation of receiving antenna height when the distance between two countries is 240 km. The propagation loss appears to have an abnormal value near the receiving antenna height of 50m and the propagation loss below the height of 75m is smaller than the free space loss 137.5dB. This result indicates that the propagation loss depends on the antenna height and the propagation loss also appears to vary according to the ducting layer height.

Fig. 6 shows the received wanted signal strength and interfering signal strength ratio at the victim receiver, road-side antenna of ITS, for variation of the time rate and propagation model. Interfering signal strength is calculated using equation (2) and the parameters in Table I and Table II. After calculating the interference power level and the wanted signal strength at the victim receiver, we can determine whether the interference occurs. The received signal-to-interference plus noise ratio appears to be dependent on the separate distance between roadside unit and vehicle unit of ITS. The target signal-to-interference plus noise ratio of 13dB may be satisfied depending on the separate distance. For 10% time rate and 50% time rate of ITU-R P.452-15 model, it satisfied the target signal-to-interference plus noise ratio in all segments. However, for a 1% time rate of ITU-R P. 452-15 model and APM, the target signal-to-interference plus noise ratio appears to be satisfied at separate distance below 150 m.

The additional attenuation loss required for the receiving antenna height of ITS's roadside is shown in Fig. 7.

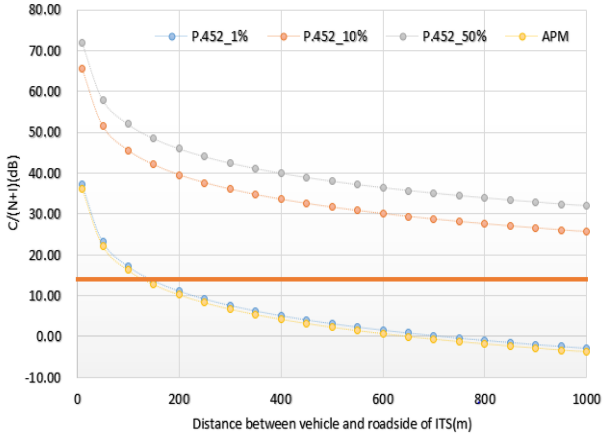

Fig. 6. Received signal-to- interference plus noise ratio according to the time rate at the roadside of ITS

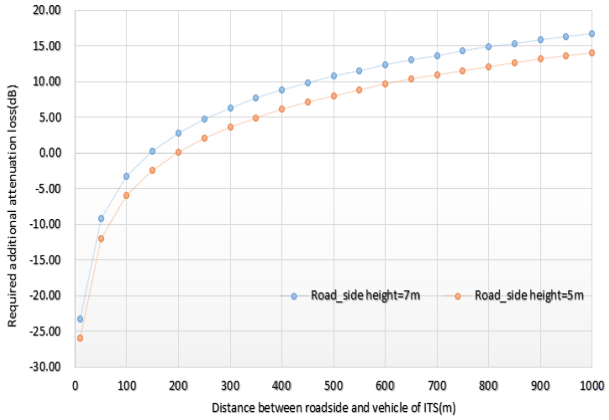

Fig. 7. Additional attenuation loss required for receiving antenna heights

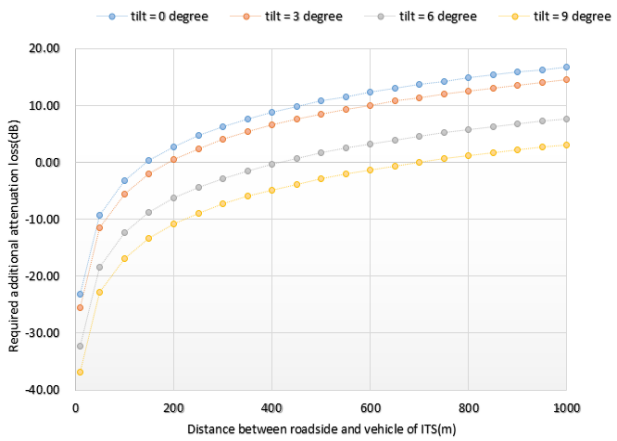

Fig. 8. Additional attenuation loss required for tilt degree of transmitting antenna

These are calculated using equation (6) and the parameters listed in Table I and Table II. When the heights of the receiving antenna of ITS's roadside is 5 m, an additional attenuation loss of above 8 dB is required to satisfy the target interference level with ITS's cell radius of 500m. As the separate distance between roadside and vehicle of ITS, cell radius, is extended, a required additional attenuation loss to satisfy the target interference level is increased. In addition, when the heights of the receiving antenna of ITS's roadside is 7 m, an additional attenuation loss of 11 dB is required. From the result, we confirm that the target interference level may be satisfied depending on the antenna height and ITS's cell radius.

Fig. 8 shows the additional attenuation loss required for variation of the tilting angle of a transmitting Korean DVB-T2 site antenna, which was simulated based on the vertical pattern of the DVB-T2 antenna in [9] and based on the APM. Also the required additional attenuation loss is compared when the tilting angle of the DVB-T2 site antenna is 0°, 3°, 6° and 9°. This result indicates that Korean DVB-T2 site system produces a higher interference on Japan's ITS system when the tilting angle of the transmitting antenna is 3° than when it is 9°.

The additional attenuation loss required, as shown in Fig. 7 and Fig. 8, can be used as a guideline for allowing the deployed Japan ITS system and Korean DVB-T2 to avoid an unacceptable amount of interference between systems.

IV. Conclusion

In this paper, we analyses the effect of interference between UHDTV services in Korea and ITS service in Japan at the 700 MHz frequency band when encountering a ducting phenomenon. The MCL method is used for an interference analysis, focusing on an interference scenario of Korea's UHDTV to Japan's ITS. The ITU-R P.452-15 model and APM were used to calculate the propagation loss in the ducts, and the modified refractivity indexes of a surface-based duct and an elevated duct as provided by a WMO station were applied. The propagation loss by ducting may be smaller than the free space loss.

The received signal-to-interference plus noise ratio and the required additional attenuation loss at Japan's ITS roadside occurring from Korea's DVB-T2 were simulated for antenna height and antenna's tilting angles. We confirmed that the strength of the received interfering signal depends on the antenna height, and that the target interference level may be satisfied by adjusting the antenna height. Also we confirmed that the received interfering signal strength depends on the transmitting antenna's tilting angles and that the target interference level may be satisfied by adjusting the tilting angle of antenna and Japan's ITS cell radius.

This paper can be used to evaluate the interference effects and find a spectrum-sharing method between Korean DVB-T2 and Japan ITS. It can also be useful for deployment planning by each system, resulting in an interference impact that is acceptable to both parties.

Acknowledgment

This work was supported by the ICT R&D program of MSIP/IITP, Republic of Korea. [B0101-15-222, Development of core technologies to improve spectral efficiency for mobile big-bang].

References

[1] Frequency policy in Korea, KICS, 5 June 2009
[2] http://www.ddaily.co.kr/news/article.html?no=132874
[3] http://english.yonhapnews.co.kr/business/2016/07/26/0504000000AEN20160726002700320.html
[4] ITU-R 5A/198-E, "WORKING DOCUMENT TOWARDS A PRELIMINARY DRAFT REVISION OF REPORT ITU-R M.2228: Advanced intelligent transport systems (ITS) radiocommunications"20 Nov. 2012
[5] H. S. Lee, "An Analysis of Radio Interference in 800MHz Band between Korea and Japan," *The Journal of Korea Information and Communication Society*, 8(1998), pp. 1952-1962.
[6] N. H. Jeong, "The Analysis of Radio Interference between Korea and China/Japan using Split-step DMFT Algorithm," *The Journal of Korea Institute of Electromagnetic Engineering and Science*, 2(2002), pp. 196-207
[7] P. Gerstoft, D. F. Gingras, L. T. Rogars, and W. S. Hodgkiss, "Estimation of Radio Refractivity Structure Using Matched-Field Array Processing," *IEEE Trans. Antennas Propagation*, 48(2000).
[8] ERC Report 101, "A comparison of the minimum coupling loss method, enhanced minimum coupling loss method, and the Monte-Carlo simulation," May, 1999.
[9] ITU-R Rec. P.452-15, "Prediction procedure for the evaluation of interference between stations on the surface of the Earth at frequencies above about 0.1GHz,"2013
[10] H. V. Hitney, "Hybrid Ray Optics and Parabolic Equation Methods for Radar Propagation Modeling," *IEE International Conference Radar 92*, 12-13, Oct. 1992.
[11] ITU-R Rec. F.1336-4, "Reference radiation patterns of omnidirectional, sectoral and other antennas for the fixed and mobile service for use in sharing studies in the frequency range from 400 MHz to about 70 GHz,"2014

Ho-Kyung Son received the B.S and M.S degrees in Electronic Engineering from Kyungpook National University, Daegu, Korea, in 1997 and 1999, and the Ph.D degree in the same university, Korea in 2013.
From March 1999 to March 2000, she was a researcher of LG Information and Communication. Since May 2000, she has been with the Electronics and Telecommunications Research Institute (ETRI), Daejeon, Korea, where she is a principal researcher of spectrum engineering research section of the Radio Technology Research Department. Her research interests include radio resource management, interference analysis between wireless communications, and radio propagation.

Young-Jun Chung received the B.S. degree from the Jeju University, Jeju Island, Korea, in 1992, and the M.S. degree in electronics engineering from Sogang University, Seoul, Korea in 1994, and Ph.D degree in Electronic Engineering from Chungnam National University, Daejeon, Korea in 2005.
Since 1994, he has been with ETRI, Daejeon, Korea, where he is a leader of spectrum engineering research and section principle member of the research staff of the Radio Technology Department. His research interests include RF circuit, RF systems, and spectrum engineering.

Analytical Description of Chromatic Dispersion Effect on Signal Propagation in the Time Domain

Mikhail Meltenisov*, Aleksandr Matukhin*

**Department of Communication Networks and Data Transmission, The Bonch-Bruevich Saint-Petersburg State University of Telecommunications, Bolshevikov Ave. 22, Saint-Petersburg, Russia*

meltenisov@gmail.com, matukhin@list.ru

***Abstract*—The investigation of chromatic dispersion effect on pulse propagation is of interest in high-speed optical transmission systems. But the chromatic dispersion effect hasn't an acceptable analytical description in the time domain. The analytical model of the dispersion effect in the time domain using a quadratic function approximation of nonlinear part of the propagation constant and the Fresnel integrals is proposed in this paper. It is shown that the obtained model is universal and it has a tunable accuracy. A simple method of estimating the memory of an optical channel is proposed. The analytical model of signal propagation in an optical channel by means of sequential generation of pairs of echo-signals is described in the article.**

***Keyword*—Analytical model, approximation, dispersion, Frensel integrals, propagation constant, time domain, echo-signal, memory of channel**

I. INTRODUCTION

AT the present time, high-speed optical transmission systems are in an active development and the investigation of the chromatic dispersion effect is one of most interest of issues. The propagation of pulses through an optical fiber, which is a dispersive medium, is well explored in [1]–[7].

$$\frac{\partial A}{\partial z}+\beta_1\frac{\partial A}{\partial t}+\frac{j\beta_2}{2}\frac{\partial^2 A}{\partial t^2}-\frac{\beta_3}{6}\frac{\partial^3 A}{\partial t^3}=0 \quad (1)$$

where $A(z,t)$ is the slowly varying pulse envelope and β_m are a parameters described in [1] .

The differential equation (1) should be solved if a pulse form in the time domain is required to find. And, this equation should be solved individually for of all kinds of pulses. Besides, a direct solution may be difficult, whereas an analytical equation is impossible to get using the fast Fourier transform. But the analytical equation may be of use in some cases, e.g. signal processing in the time domain.

In this paper, a simple and universal analytical dispersion model in the time domain will be found.

II. DISPERSION THEORY

In the Dispersion Theory [1], pulse propagation can be written in the form

$$\frac{\partial \tilde{A}}{\partial z}=-j\beta(f)\tilde{A} \quad (2)$$

where $\tilde{A}(z,f)$ is a signal spectrum at a distance *z*, and $\beta(f)$ is the propagation constant which has a frequency dependence

$$\beta(f)=\frac{2\pi f}{c}\cdot n(f) \quad (3)$$

Here, *c* is the velocity of light in vacuum and *n* is a refractive index which defined by the Sellmeier equation [8].

All nonlinear effects and the attenuation have been excluded in equation (2).

The solution of the equation is

$$\tilde{A}(z,f)=\tilde{A}(0,f)e^{-j\beta(f)z} \quad (4)$$

It completely described the effect of the chromatic dispersion on a signal.

Therefore, the transfer function of the dispersive medium is

$$H(f)=e^{-j\beta(f)z} \quad (5)$$

III. DISPERSION IN THE TIME DOMAIN

As seen from Figure 1, the propagation constant has a substantial linear part. Therefore, we can represent it as

Manuscript received October 28, 2016. This work is a follow-up of the invited journal to the conference paper of the 18th International Conference on Advanced Communication Technology (ICACT2016).

M. A. Meltenisov is with the Bonch-Bruevich Saint-Petersburg State University of Telecommunications, Saint Petersburg, Russia (corresponding author, e-mail: meltenisov@gmail.com).

A. Yu. Matukhin is with the Bonch-Bruevich Saint-Petersburg State University of Telecommunications, Saint Petersburg, Russia (e-mail: matukhin@list.ru).

$$\beta(f)=\beta_{ln}(f)+\beta_{nl}(f) \tag{6}$$

where β_{ln} is a linear part and β_{nl} is a nonlinear part of the propagation constant.

Since the entire optical spectrum is not of interest an operating band of signal will be considered further, i.e. $f\in[f_l;f_h]$ where, f_h is the higher frequency, and f_l is the lower frequency.

A. Linear Part of the Propagation Constant

The influence of β_{ln} causes signal delay in the time domain. β_{ln} can be represented in form

$$\beta_{ln}(f)=kf+p \tag{7}$$

And parameters *k* and *p* are

$$\begin{cases} k=\dfrac{\beta(f_h)-\beta(f_l)}{f_h-f_l} \\ p=\dfrac{\beta(f_l)\,f_h-\beta(f_h)\,f_l}{f_h-f_l} \end{cases} \tag{8}$$

If the nonlinear part is omitted, a pulse envelope in the time domain will be obtained in the form

$$A(z,t)=A\left(0,t-\frac{kz}{2\pi}\right)e^{-jpz} \tag{9}$$

B. Nonlinear Part of the Propagation Constant

The nonlinear part can be obtained as

$$\beta_{nl}(f)=\beta(f)-\beta_{ln}(f) \tag{10}$$

As seen from Fig. 2, it is look like quadratic function. Therefore, it can be represented as

$$\beta'_{nl}(f)=af^2+bf+c \tag{11}$$

where *a*, *b* and *c* are

$$\begin{cases} a=-4\left[\beta(f_c)-\beta_{ln}(f_c)\right]\dfrac{1}{(f_h-f_l)^2} \\ b=4\left[\beta(f_c)-\beta_{ln}(f_c)\right]\dfrac{(f_h+f_l)}{(f_h-f_l)^2} \\ c=-4\left[\beta(f_c)-\beta_{ln}(f_c)\right]\dfrac{f_h f_l}{(f_h-f_l)^2} \end{cases} \tag{12}$$

Here, f_c is a central frequency of the band.

Actually, β_{nl} is not a quadratic function. This function has some cubic part. Accordingly, there is a deviation, as shown in Fig. 3. But β_{nl} can not be approximated with a cubic function because it will obstruct further calculations.

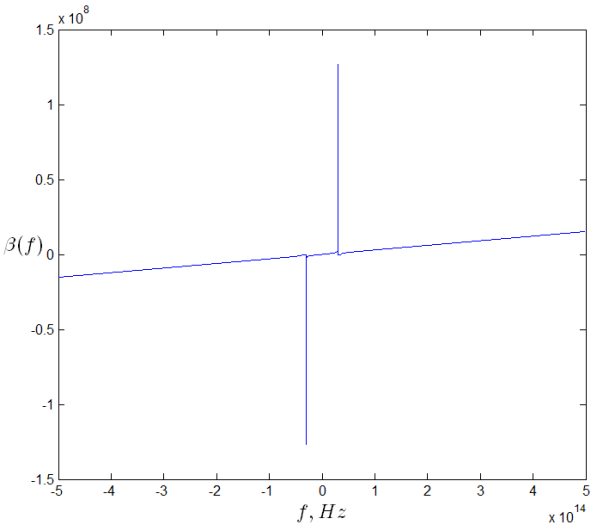

Fig. 1. Frequency dependence of the propagation constant.

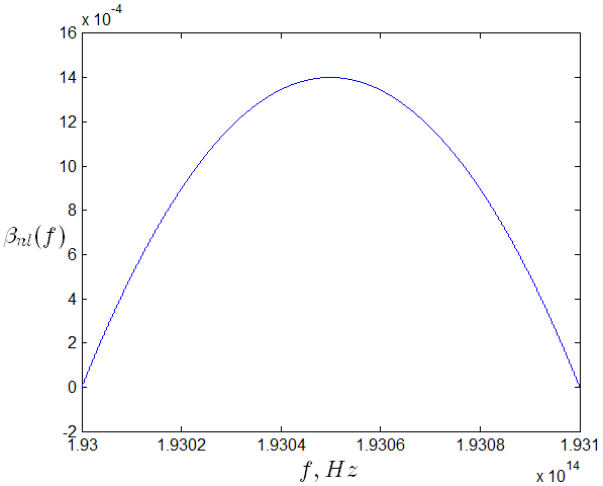

Fig. 2. A nonlinear part of the propagation constant in the 100 GHz operating band.

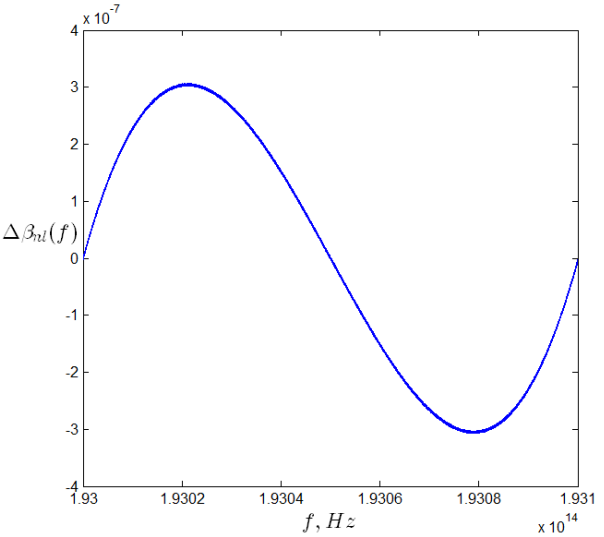

Fig. 3. An absolute error of the quadratic function approximation of nonlinear part of the propagation constant.

To minimize the deviation, the entire operating band can be divided into two. And then, the deviation function can be approximated with a quadratic function in each of sub-bands

$$\Delta\beta_{nl}(f)=\begin{cases} m_1 f^2+n_1 f+k_1,\ f\in[f_l;f_c] \\ m_2 f^2+n_2 f+k_2,\ f\in[f_c;f_h] \end{cases} \tag{13}$$

and

$$\Delta\beta_{nl}(f)=\beta_{nl}(f)-\beta'_{nl}(f) \tag{14}$$

Parameters m_1, n_1, k_1, m_2, and k_2 can be found with (12), where f_h, f_l and f_c is a higher, lower and the central frequency of the each of the ranges, respectively.

A new approximation is

$$\beta''_{nl}(f)=\begin{cases} (a+m_1)f^2+(b+n_1)f+(c+k_1),\ f\in[f_l;f_c] \\ (a+m_2)f^2+(b+n_2)f+(c+k_2),\ f\in[f_c;f_h] \end{cases} \tag{15}$$

Deviations in each of the ranges will be similar to the deviation of the first approximation. Therefore, a deviation in the entire band can be represented by four quadratic functions in four intervals.

It was found that improving of the approximation can be continued in a similar way until the error value becomes sufficient.

C. Representation of Chromatic Dispersion in the Time Domain

The transfer function of the dispersive medium can be represented as a product of two parts

$$H(f)=e^{-j\beta_{ln}(f)z}\cdot e^{-j\beta_{nl}(f)z} \tag{16}$$

First part is a linear part which described in the time domain by (9). Second part is a nonlinear part which causes a pulse distortion. Let us expand it into a Fourier series to describe it in the time domain

$$H(f)\approx e^{-j\beta_{ln}(f)z}\cdot\sum_{n=-\infty}^{\infty}c_n e^{j\frac{\pi fn}{L}} \tag{17}$$

where

$$c_n=\frac{1}{2L}\int_{f_l}^{f_h}e^{-j\beta_{nl}(f)z}e^{-j\frac{\pi fn}{L}}df \tag{18}$$

and L is a half of the entire band.

Because $\beta_{nl}(f)$ is a quadratic function c_n can be expressed in terms of the Fresnel integrals [9]

$$\begin{aligned} c_n=&\frac{e^{-j\left(\frac{(bzL+\pi n)^2}{-4azL^2}+cz\right)}}{2L\sqrt{-az}} \\ &\cdot\left[C\left(\sqrt{-az}\,f_h-\frac{bzL+\pi n}{2\sqrt{-az}L}\right)-C\left(\sqrt{-az}\,f_l-\frac{bzL+\pi n}{2\sqrt{-az}L}\right)\right. \\ &\left.+jS\left(\sqrt{-az}\,f_h-\frac{bzL+\pi n}{2\sqrt{-az}L}\right)-jS\left(\sqrt{-az}\,f_l-\frac{bzL+\pi n}{2\sqrt{-az}L}\right)\right] \end{aligned} \tag{19}$$

Here, C(x) and S(x) are the Fresnel integrals.

For second approximation of nonlinear part of the propagation constant from (15) and for next approximations, (19) should be calculated in each of sub-bands (with constant L), and the results should be summarized then.

A signal spectrum at a distance z is

$$\tilde{A}(z,j\omega)=\tilde{A}(0,j\omega)H(j\omega) \tag{20}$$

or, with (17) and (7) is

$$\tilde{A}(z,j\omega)=\sum_{n=-N}^{N}c_n e^{-jpz}\tilde{A}(0,j\omega)e^{-j\omega\left(\frac{kz}{2\pi}-\frac{n}{2L}\right)} \tag{21}$$

To describe a signal in the time domain the inverse Fourier transformation [11] should be used.

Finally, in the time domain

$$A(z,t)=\sum_{n=-N}^{N}c_n e^{-jpz}A\left(0,t+\frac{n}{2L}-\frac{kz}{2\pi}\right) \tag{22}$$

where A is a pulse envelope at a distance z and at a time moment t. L is a half of a signal bandwidth. c_n are given by (19), and p and k are given by (8).

Equation (22) describes any signal at a distance z which is distorted by the chromatic dispersion.

IV. Propagation Process in Terms of the Echo-Signals Model

Model of Chromatic Dispersion Effect (22) allows representing a signal propagation process in terms of echo-signals.

The echo-signals model [11] describes a signal at a distance z as the sum of initial signal and N pairs of lagged and anticipatory echo-signals.

$$\begin{aligned} A(z,t)=&a_0A(0,t)+\sum_{n=1}^{N}a_nA(0,t+n\tau) \\ &+\sum_{n=1}^{N}a_{-n}A(0,t-n\tau) \end{aligned} \tag{23}$$

Here, $A(0,t)$ is initial signal, $A(0,t+n\tau)$ are anticipatory echo-signals, $A(0,t-n\tau)$ are lagged

echo-signals and are some coefficients.

Expression (22) can be represented in the same form

$$A(z,t) = c_0 e^{-jpz} A\left(0, t - \frac{kz}{2\pi}\right) + \sum_{n=1}^{N} c_n e^{-jpz} A\left(0, t + \frac{n}{2L} - \frac{kz}{2\pi}\right) + \sum_{n=1}^{N} c_{-n} e^{-jpz} A\left(0, t - \frac{n}{2L} - \frac{kz}{2\pi}\right) \quad (24)$$

Here, $c_n e^{-jpz}$ corresponds to a_n, $\frac{1}{2L}$ corresponds to τ and $t - \frac{kz}{2\pi}$ corresponds to t in (23).

A. Memory of Optical Channel

The memory of channel allows estimating the number of pulses, which influence one another.

Interval between centers of two echo-signals is $\tau = \frac{1}{2L}$. Also, τ is interval between centers of two pulses. Therefore, the number of echo-signals equals the number of pulses, which influence one another. The number of echo-signals is defined by coefficients c_n, which can be called the impulse response of an optical channel if nonlinear effects are negligible. Therefore, the memory of an optical channel can be found by estimating values of c_n.

Example of the impulse response of an optical channel is shown in Fig. 4. The coefficients until certain n do not have a decreasing character and then begin decreasing rapidly.

Plotting of similar graphs allows simple finding the memory of an optical channel.

B. Propagation Process

Let us consider signal at distance *dz* at which there are two echo-signals only

$$A(dz,t) = a_0 A(0,t) + a_1 A(0, t+\tau) + a_{-1} A(0, t-\tau) \quad (25)$$

The entire line with length *z* can be divided to *N* sections with lengths *dz* as shown in Fig. 5.

Each section transforms the signal the same way as in (25): the input is $A([n-1]dz, t)$, the output is

$$A(ndz,t) = a_0 A([n-1]dz, t) + a_1 A([n-1]dz, t+\tau) + a_{-1} A([n-1]dz, t-\tau) \quad (26)$$

One section can be represented as FIR filter as shown in Fig. 6. Each section generates a new pair of echo-signals:

$$A(2dz,t) = \left[a_0^{\,2} + 2a_1 a_{-1}\right] A(0,t) + 2a_0 a_1 A(0, t+\tau) + 2a_{-1} a_0 A(0, t-\tau) + a_1^{\,2} A(0, t+2\tau) + a_{-1}^{\,2} A(0, t-2\tau) \quad (27)$$

Considering that $a_1 = a_{-1}$, signal at the distance *z* can be described by expression

$$A(Ndz,t) = \left[\sum_{k=0}^{K} c_{0k} a_0^{\,N-2k} a_1^{\,2k}\right] A(0,t) + \sum_{n=1}^{N}\left[\sum_{k=0}^{K} c_{nk} a_0^{\,N-(2k+n)} a_1^{\,2k+n}\right] A(0, t+n\tau) + \sum_{n=1}^{N}\left[\sum_{k=0}^{K} c_{nk} a_0^{\,N-(2k+n)} a_1^{\,2k+n}\right] A(0, t-n\tau) \quad (28)$$

Here, *N* is number of the sections, $K = \left\lfloor \frac{N-n}{2} \right\rfloor$ is the number of summand at *n*th echo-signal and c_{nk} are coefficients at the summands which calculated as follows

$$c_{nk} = \frac{N!}{k!(k+n)!(N-2k-n)!} \quad (29)$$

Besides, $\left[\sum_{k=0}^{K} c_{0k} a_0^{\,N-2k} a_1^{\,2k}\right]$ corresponds c_0 and $\left[\sum_{k=0}^{K} c_{0k} a_0^{\,N-2k} a_1^{\,2k}\right]$ corresponds $c_1 = c_{-1}$ from (24).

As can be seen from the above, the propagation process in an optical channel can be represented as sequential generation of pairs of echo-signals after each section with length *dz*. It could be useful for investigation of nonlinear propagation in an optical channel because the model (28) is not requires performing the Fourier transform in distinction from the split-step Fourier method [1]. All of operations are performed in time domain.

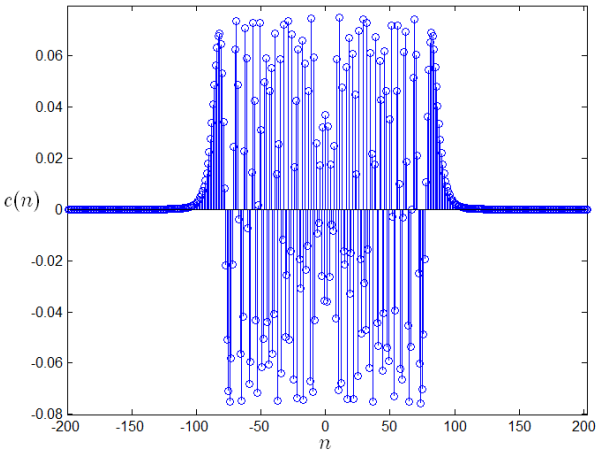

Fig. 4. The impulse response of an optical channel with 100 GHz operating band at the distance 100 km.

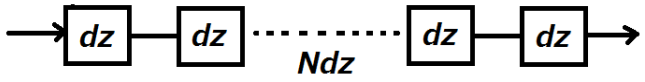

Fig. 5. The line with length *z* which is divided to *N* sections with lengths *dz*.

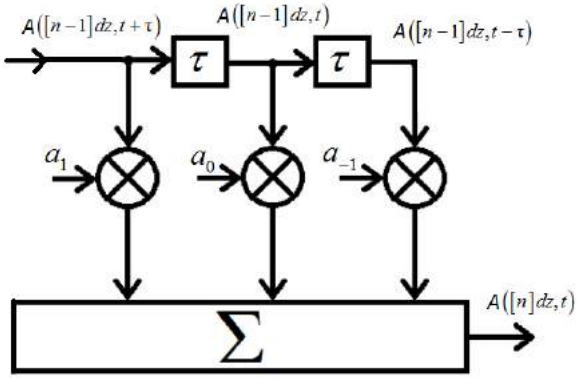

Fig. 6. Section *dz* as FIR filter.

V. Experimental Results

An accuracy of the obtained analytical model is defined by the number of the Fourier series coefficients *N* and by the number of the approximations as in (15). The first parameter is substantial in any conditions. The second is substantial only at considerable distances ≥ 1000 km and at signal bandwidths ≥ 100 GHz. Dependencies of the parameter *N* are

$$N(z) \approx z(km) \tag{30}$$

$$N(\Delta F) \approx \frac{\left[\Delta F\,(GHz)\right]^2}{100} \tag{31}$$

Some types of pulses calculated with the model are shown in Fig. 7, 8 and 9.

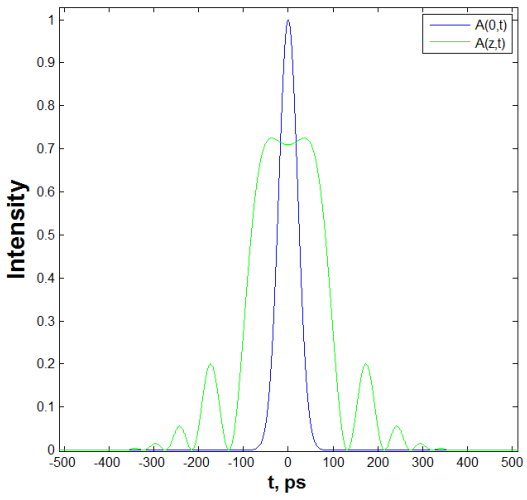

Fig. 7. Gaussian pulse with width 30 ps at the distance 155 km. The constant delay, which equaled 0.76 ms, has been compensated.

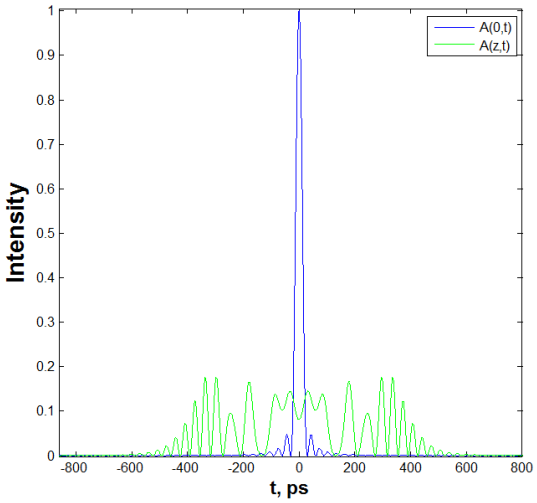

Fig. 8. Sinc pulse with width 30 ps at the distance 155 km. The constant delay, which equaled 0.76 ms, has been compensated.

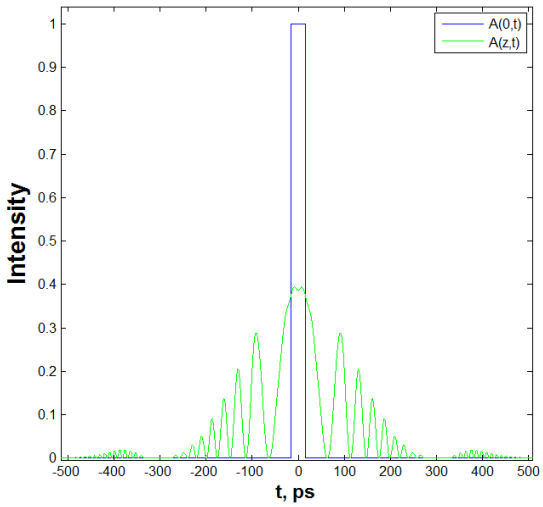

Fig. 9. Square pulse with width 30 ps at the distance 50 km. The constant delay, which equaled 0.24 ms, has been compensated.

VI. Conclusion

In this paper, an analytical model of dispersion effect in the time domain has been described. This model allows describe the chromatic dispersion effect on any signal, which propagates through optical fiber. The model has a tunable accuracy, so it is applicable in different areas such as signal propagation modeling, algorithms of dispersion compensation, etc.

It has been shown that the propagation process in an optical channel can be represented as sequential generation of pairs of echo-signals. The model is an analytical and described in time domain. The applications of this model are an optical signal propagation modeling which includes the nonlinear propagation and algorithms of dispersion compensation.

Furthermore, the method of estimating the memory of an optical channel is proposed in this article. It requires only the estimation of values of coefficients at each echo-signal.

A problem of the proposed models is a high computational complexity in the case of wide signal bandwidths and considerable distances. However, the main task of this model is the using it in an analytical equations. In this case, the computational complexity is not substantial.

REFERENCES

[1] G. P. Agrawal, *Nonlinear Fiber Optics* (5th ed.), New York: Academic, 2013.

[2] S. J. Orfanidis. (2016, August 1). *Electromagnetic Waves and Antennas* [Online]. Available: http://www.ece.rutgers.edu/~orfanidi/ewa

[3] E. Iannone, F. Matera, A. Mecozzi, and M. Settembre, *Nonlinear Optical Communication Networks*, New York: Wiley, 1998.

[4] S. Elahmadi, M. D. Srinath, D. Rajan, and R. Haberman, *Capacity and Modeling of Nonlinear Fiber Optic Communications as a Frequency-Selective Fading Channel*, in *Proc. ICNC'12*, 2012.

[5] K. N. Modi, *Modeling, Detection and Signal Design for Multichannel Fiber Optic Communications*, Univ. of Virginia, 2009.

[6] R. Gaudino, and E. Viterbo, "Pulse shape optimization in dispersion-limited direct detection optical fiber links", *IEEE Communications Lett.*, vol.7, pp. 552–554, Nov. 2003.

[7] K. Kashiwagi, H. Ishizu, and T. Kurokawa, "Fiber Transmission Characteristics of Parabolic Pulses Generated by Optical Pulse Synthesizer," *Japanese Journal of Applied Physics*, vol. 50, Sep. 2011.

[8] M. J. Adams, *An Introduction to Optical Waveguides*, New York: Wiley, 1981.

[9] Y. Luke, *Mathematical Functions and Their Approximations*, New York: Academic Press, 1975.

[10] N. Morrison, *Introduction to Fourier Analysis*, New York: Wiley, 1994.

[11] N. N. Baeva, I. K. Bobrovskaya, V. A. Breskin., Yu. A. Yakub, *Fundamentals of multi-channel communication. Textbook for High Schools*, Moskow: Svyaz, 1975, (in Russian)

Mikhail A. Meltenisov was born in Russia in 1989. He graduated the Bonch-Bruevich Saint-Petersburg State University of Telecommunications, Russia as the engineer at specialty "multichannel transmission systems" and as the master at area "infocommunication technologies and telecommunication systems" in 2011 and 2013, respectively. In 2013, he took a postgraduate course on specialty "systems, networks and telecommunications devices" in the same university.

He is working in St.Petersburg University of Telecommunication as Research Engineer since 2015. His studies focused on adaptive signal processing in fiber optic transmission systems.

Dr. Aleksandr Matukhin was born in 1973 in USSR. He graduated Bonch-Bruevich Saint-Petersburg State University of Telecommunications, Russia as the engineer at specialty "multichannel transmission systems" in 1996. He received Ph.D from St.Petersburg University of Telecommunication in 2004.

He worked in St.Petersburg University of Telecommunication as assistant, senior lecturer, associate professor and chief Department of Multichannel Transmission Systems since 1997. Now he is working in St.Petersburg University of Telecommunication as Associate Professor Department of Communications Networks. His studies focused on adaptive signal processing in multichannel transmission systems.

Dynamic Analysis of Rotor Blade System

Liu Yi

School of Aerospace Engineering, Beijing Institute of Technology, Beijing, China

bjliuyi_2015@163.com

***Abstract*—To make the rotation of the rotor blade more accurate, the elastic deformation in the system is considered in this paper. Firstly, the number and direction of the generalized coordinates are determined by the freedom degree of the blade and the finite element method and Lagrange equation are used to build the dynamical equation of the rotor blade system. Then, we obtain the position vector, the mass matrix, the derivative of Mass Matrix on time and other coefficient matrix according to the principle of flexible multibody dynamics. Finally, the violation correction method is used to get the numerical solution of the dynamical equation in the simulation. Additionally, the angular displacement of the hub around the main axis, the angular displacement of the blade end and elastic deformation in the y-direction and z-direction are analyzed to prove the correctness of the model.**

***Keyword*—rotor blade, elastic deformation, finite element, flexible multibody dynamics.**

I. INTRODUCTION

THE study of flexible multibody dynamics began in the late 1950s during which the US launched the first artificial satellite. In the past 20 years, due to its very close relationship with the engineering field, such as aerospace, aviation, machinery, vehicles and robots, even with the sports, flexible multibody dynamics have caused great concern and become an active study field of theoretical and applied mechanics. Flexible multibody dynamics researches the dynamics behavior of the systems consisted of deformable objects and rigid body during wide-range spatial movement. Flexible multibody dynamics focus on "flexible", and study the interaction between the objects' deformation and overall rigidity movement. The character that deformation movement and rigidity movement occur and couple simultaneously is the core feature of flexible multibody dynamics.

A novel mathematical formulation capable of treating the problems of maneuvering and control of flexible multibody structures is developed [1]. The authors focused on an approach to the study of the dynamics and control of large flexible space structures which comprised of subassemblies, a subject of considerable contemporary interest [2]. A flexible multibody dynamics formulation to analyze the vibration of hard disk drives is presented [3-4]. The inverse-dynamic model of mobile multibody systems articulated with joints and wheels is built and an easily implementable algorithm which is based on Newton–Euler recursive dynamics is proposed [5]. This authors presented several iterative algorithms regarding the dynamic analysis of multibody systems [6].

However, there is few literatures investigating the dynamic of the rotor blade using the flexible multibody dynamics. Moreover, the research on helicopter fall behind that on Fixed-wing aircraft, the reason is mainly that the awareness of the helicopter rotor aerodynamic is not sufficient. Based on this, the dynamical equation of the rotor blade system is built using the finite element method and the Lagrange equation. Additionally, the mass matrix and other coefficient matrix are obtained. After that, the simulation is used to verify the correctness of the dynamical model.

II. SYSTEM MODEL

Helicopter rotor is composed of hub and several blades. The hub mounted on the rotor shaft, while the blade which likes the slender wing connects to the hub. The hub and blade rotated together with the helicopter engine rotation, and the interaction between the blade and the surrounding air can create the thrust along the rotor shaft. Additionally, the blade contains flap, lag and torsion, and all these motions coupled together to formed a complex structure-dynamics problem.

The helicopter rotor not only rotates around the engine shaft, but also has Elastic deformations due to its flexible. According to the motion characteristics of the rotor blade in space, we can determine the number of generalized coordinates, and build the finite element model of the rotor blade in Fig. 1.

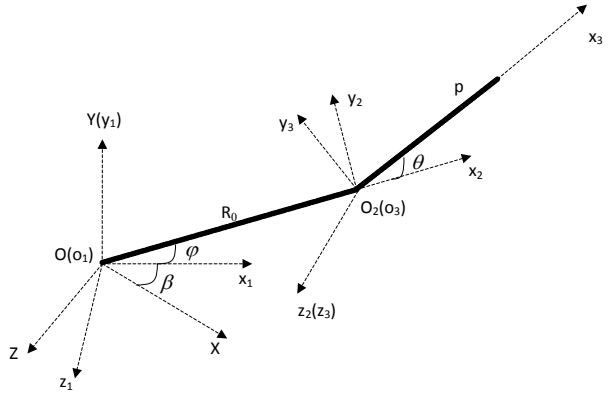

Fig. 1. The finite element model of the rotor blade.

In Fig. 1, OXYZ is the inertial coordinate frame, while $o_1x_1y_1z_1$, $o_2x_2y_2z_2$ and $o_3x_3y_3z_3$ are the moving coordinates. The $o_1x_1y_1z_1$ frame rotates around OY axis with vector R_0,

Manuscript received October 19, 2016. This work is a follow-up of the invited journal to the accepted conference paper of the 18th International Conference on Advanced Communication Technology (ICACT2016)

Liu Yi is with School of Aerospace Engineering, Beijing Institute of Technology, Beijing, China (corresponding author's phone: +86-15011440975; e-mail: bjliuyi_2015@163.com).

and the rotation angle is β; the $o_2x_2y_2z_2$ frame rotates around o1z1 axis with vector R_0 , and the rotation angle is β; the $o_3x_3y_3z_3$ frame whose origin coincides with that of the $o_1x_1y_1z_1$ frame rotates around o_2z_2 axis with vector R_0 , and the rotation angle is θ.

III. DYNAMICAL EQUATION AND COEFFICIENT MATRIX OF THE ROTOR BLADE

A. Dynamical Equation

The dynamical equation of flexible multibody systems is given as follows:

$$M\ddot{q}+\dot{M}\dot{q}-\frac{1}{2}\dot{q}^{T}\frac{\partial M}{\partial q}\dot{q}+Kq=Q_F \tag{1}$$

In helicopter rotor system, the blade is hinge connected to the hub, and flap around the hub. The hub rotates around the engine shaft. Due to the damping effect in these motions, the damping coefficient matrix and the constraint equation are introduced, and dynamical equation of the helicopter rotor blade can be written as follows:

$$M\ddot{q}+D\dot{q}+Kq+C_q^T\lambda=Q_F+Q_V \tag{2}$$

where M is the mass matrix, Q_F is the generalized external force vector, q is the generalized coordinate vector, $\dot{q}$ is the generalized speed vector, D is the damping coefficient matrix, K is the stiffness coefficient matrix, C_q is the constraint Jacobian matrix, λ is the Lagrange multipliers vector, and $C_q^T\lambda$ is the generalized constraint force.

Submitting $Q_V=-\dot{M}\dot{q}+\frac{1}{2}\dot{q}^{T}(\frac{\partial M}{\partial q})\dot{q}$ into Equation (2), the dynamical equation can be rewritten as:

$$M\ddot{q}+(D+\dot{M})\dot{q}+Kq+C_q^T\lambda=Q_F+\frac{1}{2}\dot{q}^{T}(\frac{\partial M}{\partial q})\dot{q} \tag{3}$$

Where $\dot{M}$ is the partial derivative of mass matrix on time, $\frac{\partial M}{\partial q}$ is the derivative of mass matrix on generalized coordinate.

B. Position Vector

The displacement of the arbitrary point on beam element in the inertial coordinate frame can be given as

$$R_p=R_0+A_1A_2A_3(u_0+Nq_f) \tag{4}$$

where $R_p=[x_0 \quad y_0 \quad z_0]$ is the position at the start time, $A_1=\begin{bmatrix}\cos\beta & 0 & \sin\beta\\ 0 & 1 & 0\\ -\sin\beta & 0 & \cos\beta\end{bmatrix}$ is the rotation matrix from $o_1x_1y_1z$ to OXYZ, $A_2=\begin{bmatrix}\cos\varphi & -\sin\varphi & 0\\ \sin\varphi & \cos\varphi & 0\\ 0 & 0 & 1\end{bmatrix}$ is the rotation matrix from $o_2x_2y_2z_2$ to OXYZ, $A_3=\begin{bmatrix}\cos\theta & -\sin\theta & 0\\ \sin\theta & \cos\theta & 0\\ 0 & 0 & 1\end{bmatrix}$ is the rotation matrix from $o_3x_3y_3z_3$ to OXYZ, β is the rotation angle around OY axis, φ is the rotation angle around oz_1 axis, θ is the rotation angle around o_2z_2 axis, u is the vector of point p after distortion in moving coordinates $o_3x_3y_3z_3$, u_0 is the vector of point p without distortion in moving coordinates $o_3x_3y_3z_3$, and is the position vector of point p by distortion in moving coordinates $o_3x_3y_3z_3$.

The flight conditions of helicopter is different with different β, φ and θ. The state of analysis in this paper is as shown in formula (4). At this time, the helicopter fly forward, backward, or fly by hover. When $\beta=0$, the helicopter is in a static state; when β is a fixed value and $\varphi=0$, the helicopter is in the air hover state; when β and φ are both constant, the helicopter in the air flight state.

According to the finite element principle [7-8], the displacement of any point on the element can be represented using the interpolation method. That is, the displacements of the element nodes are used to represent the elastic deformation at any point on the element.

Setting u_0 as the position vector before beam deformation, N as the shape function of beam element, and q_f as displacement vector of beam element, the elastic deformation at any point on the element can be given as follows:

$$N_f=Nq_f \tag{5}$$

where

$$N_f=\begin{bmatrix}n_1 & 0 & 0 & 0 & 0 & 0 & n_2 & 0 & 0 & 0 & 0 & 0\\ 0 & n_3 & 0 & 0 & 0 & n_4 & 0 & n_5 & 0 & 0 & 0 & n_6\\ 0 & 0 & n_3 & 0 & n_7 & 0 & 0 & 0 & n_5 & 0 & n_8 & 0\end{bmatrix}$$ is the shape function of beam element, and $n_1=1-\frac{x}{l}$, $n_2=\frac{x}{l}$, $n_3=1-\frac{3x^2}{l^2}+\frac{2x^3}{l^3}$, $n_4=x-\frac{2x^2}{l}+\frac{x^3}{l^2}$, $n_5=\frac{3x^2}{l^2}-\frac{2x^3}{l^3}$, $n_6=-\frac{3x^2}{l}+\frac{x^3}{l^2}$, $n_7=-n_4$, $n_8=-n_6$, x is the abscissa of any point in moving coordinates $o_3x_3y_3z_3$, l is the length of the beam element.

Space beam element has two nodes (i node and j node), each node has six degrees of freedom along the three coordinate axes and three axes around the rotation, thus the node displacement vector can be expressed as

$$q_f=\begin{bmatrix}q_{i1} & q_{i2} & q_{i3} & q_{i4} & q_{i5} & q_{i6} & q_{j1} & q_{j1} & q_{j1} & q_{j1} & q_{j1} & q_{j1}\end{bmatrix}^T$$

C. Mass Matrix

Calculating the derivative on time in equation (4), we can get the speed of point p as follows:

$$\begin{aligned}\dot{R}_p=\dot{R}_0+A_{1\beta}\dot{\beta}A_2A_3U+A_1A_{2\varphi}\dot{\varphi}A_3U\\ +A_1A_2A_{3\theta}\dot{\theta}U+A_1A_2A_3N\dot{q}_f\end{aligned} \tag{6}$$

Due to the constant u_0, we can get $\dot{u}_0=0$ and $\dot{u}=N\dot{q}_f$. Base on this, the equation (6) can be reorganized as:

$$\dot{R}_p = [I \;\; A_1\beta A_2 A_3 U \;\; A_1 A_2\varphi A_3 U \;\; A_1 A_2 A_3\theta U \;\; A_1 A_2 A_3 N] \begin{bmatrix} \dot{R}_0 \\ \dot{\beta} \\ \dot{\varphi} \\ \dot{\theta} \\ \dot{q}_f \end{bmatrix} \quad (7)$$

where $\dot{R}_p$ is the velocity vector at any point on the beam, $\dot{q}_f$ is the derivative of beam element's displacement on time, $A_{3\theta} = \begin{bmatrix} -\sin\theta & -\cos\theta & 0 \\ \cos\theta & -\sin\theta & 0 \\ 0 & 0 & 0 \end{bmatrix}$ is the derivative of A_3 on θ, $A_{1\beta} = \begin{bmatrix} -\sin\beta & 0 & \cos\beta \\ 0 & 0 & 0 \\ -\cos\beta & 0 & -\sin\beta \end{bmatrix}$ is the derivative of A1 on β, $A_{2\beta} = \begin{bmatrix} -\sin\varphi & -\cos\varphi & 0 \\ \cos\varphi & -\sin\varphi & 0 \\ 0 & 0 & 0 \end{bmatrix}$ is the derivative of A2 on φ, $\dot{q} = \begin{bmatrix} \dot{R}_0 & \dot{\beta} & \dot{\varphi} & \dot{\theta} & \dot{q}_f \end{bmatrix}^T$ is the generalized velocity vector.

The kinetic energy of the flexible body is given as:

$$T = \frac{1}{2}\int_V \rho \dot{R}_p^T \dot{R}_p \, dV = \frac{1}{2}\dot{q}^T M \dot{q} \quad (8)$$

where ρ and V are the density and volume of the beam element respectively.

Submitting Equation (7) into Equation (8), we can kinetic energy can be rewritten as:

$$\begin{aligned} T &= \frac{1}{2}\int_V \rho \dot{R}_p^T \dot{R}_p \, dV \\ &= \frac{1}{2}\int_V \dot{q}^T \begin{bmatrix} I \\ A_{1\beta}A_2A_3U \\ A_1A_{2\varphi}A_3U \\ A_1A_2A_{3\theta}U \\ A_1A_2A_3N \end{bmatrix} [I \;\; A_{1\beta}A_2A_3U \;\; A_1A_{2\varphi}A_3U \;\; A_1A_2A_{3\theta}U \;\; A_1A_2A_3N] \dot{q} \, dV \\ &= \frac{1}{2}\dot{q}^T M \dot{q} \end{aligned} \quad (9)$$

From Equation (8), the mass matrix of the rotor blade M can be obtained.

D. The derivative of Mass Matrix on time

The derivative of mass matrix on time is given as follows:

$$\dot{M} = \frac{\partial M}{\partial q}\frac{\partial q}{\partial t} = \frac{\partial M}{\partial q}\dot{q} \quad (10)$$

Since β, θ, and φ all contains one generalized coordinate, q_f has 12 generalized coordinates, and R_0 has three generalized coordinates, $\dot{q}$ can be written as

$$\dot{q} = \begin{bmatrix} \dot{X}_0 & \dot{Y}_0 & \dot{Z}_0 & \dot{\beta} & \dot{\varphi} & \dot{\theta} & \dot{q}_{i1} & \dot{q}_{i2} & \dot{q}_{i3} \\ \dot{q}_{i4} & \dot{q}_{i5} & \dot{q}_{i6} & \dot{q}_{j1} & \dot{q}_{j2} & \dot{q}_{j3} & \dot{q}_{j4} & \dot{q}_{j5} & \dot{q}_{j6} \end{bmatrix} \quad (11)$$

The generalized coordinate is vector, thus the above equation is the partial derivative of the mass matrix on each generalized coordinate. Based on this, the derivative of mass matrix on time can be rewritten as

$$\dot{M} = \sum_{i=1}^{18}\frac{\partial M}{\partial q_i}\dot{q}_i = \begin{bmatrix} \dot{m}_{11} & \dot{m}_{12} & \dot{m}_{13} & \dot{m}_{14} & \dot{m}_{15} \\ & \dot{m}_{22} & \dot{m}_{23} & \dot{m}_{24} & \dot{m}_{25} \\ & & \dot{m}_{33} & \dot{m}_{34} & \dot{m}_{35} \\ & & & \dot{m}_{44} & \dot{m}_{45} \\ & & & & \dot{m}_{55} \end{bmatrix} \quad (12)$$

where

$$\frac{\partial M}{\partial q_i} = \begin{bmatrix} \frac{\partial m_{11}}{\partial q_i} & \frac{\partial m_{12}}{\partial q_i} & \frac{\partial m_{13}}{\partial q_i} & \frac{\partial m_{14}}{\partial q_i} & \frac{\partial m_{15}}{\partial q_i} \\ & \frac{\partial m_{22}}{\partial q_i} & \frac{\partial m_{23}}{\partial q_i} & \frac{\partial m_{24}}{\partial q_i} & \frac{\partial m_{25}}{\partial q_i} \\ & & \frac{\partial m_{33}}{\partial q_i} & \frac{\partial m_{34}}{\partial q_i} & \frac{\partial m_{35}}{\partial q_i} \\ & & & \frac{\partial m_{44}}{\partial q_i} & \frac{\partial m_{45}}{\partial q_i} \\ & & & & \frac{\partial m_{55}}{\partial q_i} \end{bmatrix},$$

$$\dot{m}_{11} = \sum_{i=1}^{18}\frac{\partial m_{11}}{\partial q_i}\dot{q}_i \quad ,$$

$$\dot{m}_{12} = \dot{m}_{21} = \sum_{i=1}^{18}\frac{\partial m_{12}}{\partial q_i}\dot{q}_i, \dot{m}_{13} = \dot{m}_{31} = \sum_{i=1}^{18}\frac{\partial m_{13}}{\partial q_i}\dot{q}_i,$$

$$\dot{m}_{14} = \dot{m}_{41} = \sum_{i=1}^{18}\frac{\partial m_{14}}{\partial q_i}\dot{q}_i, \; \dot{m}_{15} = \dot{m}_{51} = \sum_{i=1}^{18}\frac{\partial m_{15}}{\partial q_i}\dot{q}_i,$$

$$\dot{m}_{22} = \sum_{i=1}^{18}\frac{\partial m_{22}}{\partial q_i}\dot{q}_i, \; \dot{m}_{23} = \dot{m}_{32} = \sum_{i=1}^{18}\frac{\partial m_{23}}{\partial q_i}\dot{q}_i,$$

$$\dot{m}_{24} = \dot{m}_{42} = \sum_{i=1}^{18}\frac{\partial m_{24}}{\partial q_i}\dot{q}_i, \; \dot{m}_{25} = \dot{m}_{52} = \sum_{i=1}^{18}\frac{\partial m_{25}}{\partial q_i}\dot{q}_i,$$

$$\dot{m}_{33} = \sum_{i=1}^{18}\frac{\partial m_{33}}{\partial q_i}\dot{q}_i, \; \dot{m}_{34} = \sum_{i=1}^{18}\frac{\partial m_{34}}{\partial q_i}\dot{q}_i, \; \dot{m}_{35} = \sum_{i=1}^{18}\frac{\partial m_{35}}{\partial q_i}\dot{q}_i,$$

$$\dot{m}_{44} = \sum_{i=1}^{18}\frac{\partial m_{44}}{\partial q_i}\dot{q}_i, \; \dot{m}_{45} = \sum_{i=1}^{18}\frac{\partial m_{45}}{\partial q_i}\dot{q}_i, \; \dot{m}_{55} = \sum_{i=1}^{18}\frac{\partial m_{55}}{\partial q_i}\dot{q}_i.$$

E. Partial Derivatives of Kinetic Energy on Generalized Coordinates

Based on the expression of kinetic energy in equation (9), the partial derivative of kinetic energy on the generalized coordinate can be expressed as

$$\frac{\partial T}{\partial q} = \frac{1}{2}\dot{q}^T \frac{\partial M}{\partial q}\dot{q} = \begin{bmatrix} \frac{1}{2}\dot{q}^T \frac{\partial M}{\partial q_1}\dot{q} \\ \cdots\cdots \\ \frac{1}{2}\dot{q}^T \frac{\partial M}{\partial q_{18}}\dot{q} \end{bmatrix} \quad (13)$$

F. Constraint Equation and Jacobian Matrix

The Lagrange multipliers method is used to build the constraint equation in this paper. The general form of the constraint equation is $C(q,t) = 0$. The distance between the

blade root and the rotation center is constant, thus the constraint equation of the rotation center is given as:

$$C(q,t) = R_0 + A_1A_2A_3u_f^i - l_0 \tag{14}$$

where R_0 is the position vector of the rotation center, u_f^i is the elastic deformation, l_0 is the distance between the blade root and the rotation center.

According the relationship of the location change between each object, the constraint equation with variational form can be obtained as $C_q\delta q = 0$. Then, the constraint Jacobian matrix can be derived as：

$$C_q = \begin{bmatrix} c_{11} & \bullet & \bullet & c_{1n} \\ \bullet & \bullet & \bullet & \bullet \\ \bullet & \bullet & \bullet & \bullet \\ c_{m1} & \bullet & \bullet & c_{mn} \end{bmatrix} \tag{15}$$

where $c_{ij} = \frac{\partial c_i}{\partial q_i}$, m is the number of the constraint equations, n is the number of generalized coordinate. In multibody system, the element C_q is the the partial derivative of the i-th constraint equation on the j-th generalized coordinate.

G. Stiffness Matrix

The virtual work of the cell in the object can be written as:

$$\delta W = -\int_V \sigma^T \delta\varepsilon dV \tag{16}$$

where σ and ε are the stress and strain. For the linear isotropic materials, we can get $\sigma = E_T\varepsilon$, where E_T is the elastic quantity matrix. The strain can be got by $\varepsilon = Du_f = DNq_f$, where D is the partial differential operators of the strain-displacement.

Submitting the expression ofεinto equation (17), the virtual work can be rewritten as:

$$\delta W = -q_f^T K_{ff}\delta q_f \tag{17}$$

From the equation (17), the beam element stiffness matrix can be derived as:

$$K_{ff} = \int (DN)^T EDNdV \tag{18}$$

H. Damping Matrix

The aerodynamics model is two-dimensional steady model in this paper. The introduction of damping coefficient has two functions. One is to balance the torque of the helicopter engineer to make the rotor shaft uniform rotation. The other is supporting a big attenuation coefficient to the flap of the blade, increase the iterative rate of the flap and reduce the computation time.

The damping coefficients of the rotor shaft and flapping ream are $D_{\theta\theta}$ and $D_{\beta\beta}$ respectively, then the damping matrix of the system can be written as $D = diag(0\ D_{\theta\theta}\ D_{\beta\beta}\ 0)$, where $diag(\bullet)$ denotes the diagonal matrix.

IV. SIMULATION

In this section, the simulation is used to verify the model built in the section above. The MATLAB software is used to solve the dynamical equation. The rotor type in the simulation is OA212-207, and the main parameters are shown in Table 1.

The initial values are as follows: the rotor shaft rotates with the speed of 36.63rad/s, the elastic deformation is 0, the initial acceleration can be derived by $\ddot{q}_0 = M_0^- Q_{F0}$, where M0 is the initial mass matrix, Q_{F0} is the initial generalized external force.

In the simulation, the viscous damping is used to simulate the air friction within Rotating surface of the rotor blade. The mass matrix, partial derivative of mass matrix on time, partial derivative of mass matrix on generalized coordinate, stiffness matrix, damping matrix are input to matlab, and the violation correction method is used to get the numerical solution of the dynamical equation. The Iterative step is 10^{-4}, and the iterative time is 2s.

TABLE I
MAIN PARAMETERS

Parameter	Value
Deadweight	M=1975kg
Radius of the rotor	l=5.5m
Number of the blades	n=4
Torsion	Fz=35000N/m
Moment of Inertia on blade	Iz=6726kg/m
Stiffness coefficient of torsion	$k_\beta = 18000N/m$
Damping coefficients of the rotor shaft	$D_{\theta\theta}$=1600
Radius of the hub	r=0.5m

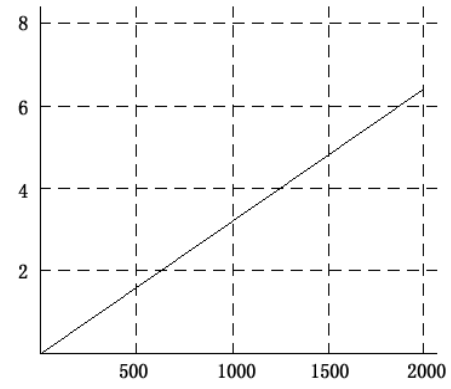

Fig. 2. The Curve of β

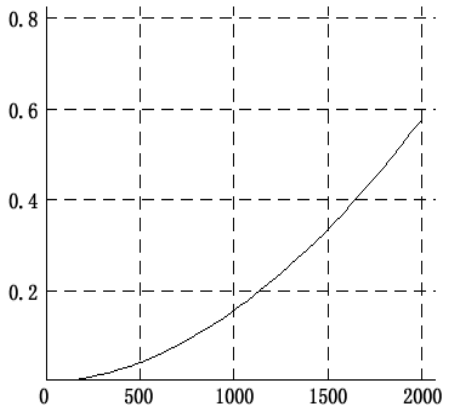

Fig. 3. The Curve of φ

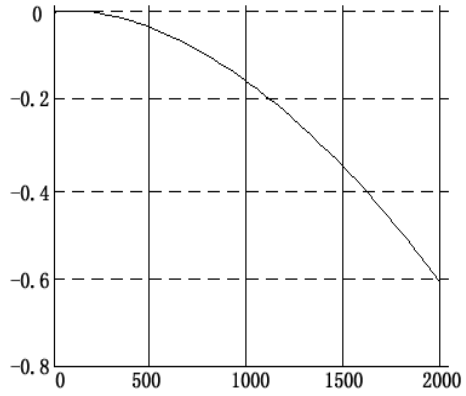

Fig. 4. The Curve of θ

Fig. 2 shows the angular displacement of the hub around the main axis. The angular displacement of the hub is a straight line, and the rotational speed descends slowly with small oscillation. Fig. 3 shows the angular displacement of the hub around dynamic axis and Fig. 4 shows the angular displacement of the impeller around dynamic axis. It can be seen that the two angular displacements are quadratic. At the end of time t = 2s, the angular displacement of the hub around the dynamic axis and the angular displacement of the impeller around dynamic axis are both agreement with the expected results, which indicates that the coordinate transformation matrix theory in this paper is correct.

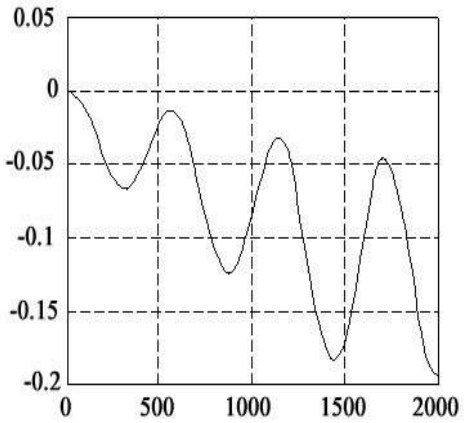

Fig. 5. Angular displacement with in the y-direction

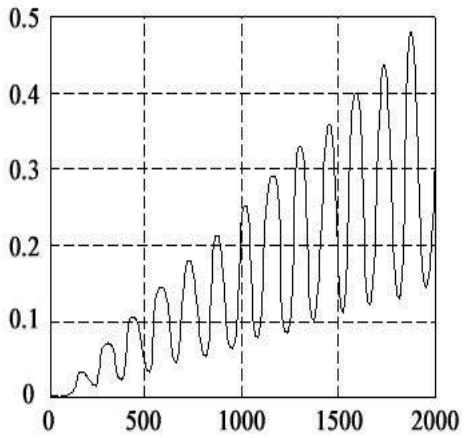

Fig. 6. Deformation with in y-direction

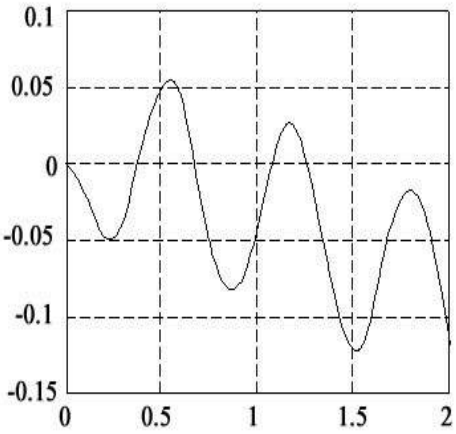

Fig. 7. Angular displacement with in the z-direction

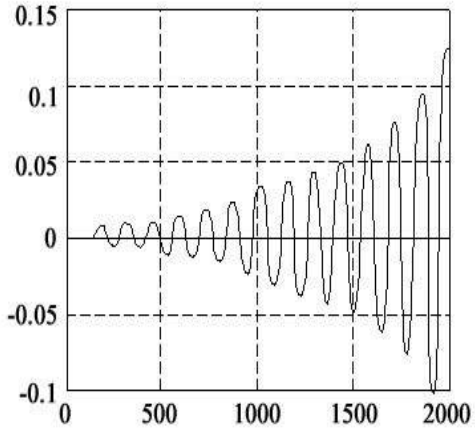

Fig.8. Deformation with in z-direction

Fig. 5 and Fig. 7 show the angular displacement of the blade end with in the y-direction and z-direction respectively, and Fig. 6 and Fig. 8 show the deformation of the blade end with in y-direction and z-direction respectively. From these figures, we can see that the a certain elastic deformation of the blade emerges due to its elasticity during the rotation of the rotor blade, and the elastic deformation can make the blade end deviates from a predetermined trajectory which will affect the positioning accuracy. Thus, the elastic deformation should be considered to make the rotational of the blade more accurate in practice. The vertical vibration cycle of the blade end in the plane which is perpendicular to the rotation plane is one seventeenth of that of the rotor shaft, and has lower frequency than that of the blade end in the rotation plane. These verify that the theoretical formula in this paper is correct.

V. CONCLUSION

The dynamical equation of the helicopter rotor blade system is built based on the finite element method and the Lagrange equation. Also, the mass matrix and its derivative on time are obtained based on the flexible multibody dynamics. In the simulation, the violation correction method is used to get the numerical solution of the dynamical equation. Simultaneously, the angular displacement of the hub around the main axis, the angular displacement of the blade end and elastic deformation in the y-direction and z-direction are got

and analyzed to verify that the model in this paper is correct.

REFERENCES

[1] Yen, Gary G., and Moon K. Kwak, "Dynamic modeling of flexible multibody structures," *IEEE Transactions on Aerospace and Electronic Systems*, 35.1 (1999): 148-156.

[2] Grewal, A., and V. J. Modi, "Multibody dynamics and robust control of flexible spacecraft," *IEEE Transactions on Aerospace and Electronic Systems*, 36.2 (2000): 491-500.

[3] Gao, Feng, Fook Fah Yap, and Ying Yan,"Modeling of hard disk drives for vibration analysis using a flexible multibody dynamics formulation." *IEEE Transactions on Magnetics*, 41.2 (2005): 744-749.

[4] Liu, Mengjun, Fook Fah Yap, and Hendri Harmoko, "A model for a hard disk drive for vibration and shock analysis," *IEEE Transactions on Magnetics*, 44.12 (2008): 4764-4768.

[5] Boyer, Frédéric, and Shaukat Ali, "Recursive inverse dynamics of mobile multibody systems with joints and wheels," *IEEE Transactions on Robotics*, 27.2 (2011): 215-228.

[6] Sun, Wei, Xiao-Guang Fan, and Tong Wang, "Efficient Iteration methods for Constrained Multibody Dynamics & Symposia," *11th IEEE International Conference on Control & Automation (ICCA)*, 2014.

[7] Brezzi, Franco, and Michel Fortin. Mixed and hybrid finite element methods. Vol. 15. *Springer Science & Business Media*, 2012.

[8] Zienkiewicz, Olgierd Cecil, and Robert Leroy Taylor. The finite element method: solid mechanics. Vol. 2. *Butterworth-heinemann*, 2000.

Liu Yi , born on 1993-01-03 in Beijing, is a senior student in Beijing Institute of Technology, Beijing, China. The major is Engineering Mechanics.

His current research interests mainly include multibody dynamics, mechanism modeling and system identification modeling. And he has published two conference papers.

Formulating Closeness Centralities on Workflow-supported Performer-Activity Affiliation Networks

Hyunah Kim*, Kwanghoon Pio Kim*
*Dept. of Computer Science, KYONGGI UNIVERSITY, Suwonsi Kyonggido, Republic of Korea
hyuna2486@naver.com, kwang@kgu.ac.kr

***Abstract*—This paper focuses on a special type of enterprise social networks, which is called 'workflow-supported activity-performer affiliation network,' and particularly formulates a metric of closeness centrality to numerically analyze the degree of clerical familiarities among performers who are involved in a workflow-supported activity-performer affiliation network. A workflow model specifies enactment sequences of the associated activities and their affiliated relationships with roles, performers, invoked-applications, and relevant data. These affiliated relationships can be revived into valuable organizational knowledge supporting business intelligence as well as managerial decision-making activities. In this paper, we particularly focus on formulating the affiliated relationships between activities and performers in a workflow model to numerically measure the closeness centralities of performers as well as the closeness centralities of activities. We also devise a series of algorithms for implementing the formulated closeness centrality equations, and describe the ultimate implications of these closeness centrality formulations in workflow-supported organizations.**

***Keywords*-workflow-supported affiliation network, ICN-based workflow model, organizational closeness centrality, business process intelligence**

I. Introduction

In recent, the workflow literature starts being interested in re-positioning the traditional workflow systems into the tools of business and organizational knowledge and intelligence. It begins from the strong belief that social relationships and collaborative behaviors among workflow-performers obviously affect the overall performance and being crowned with great successes in the real businesses and the working productivity as well. The typical pioneering outcomes of those re-positioning works ought to be [1][2][3], in which the authors formalize mechanisms and their related algorithms to discover workflow-supported social networking knowledge from workflow models and their enactment event logs. In general, the workflow model is formally defined by using the information control net (ICN)[4] methodology. In defining a workflow model, we have to specify four types of the performer-centered affiliation relationships[5] by associating each individual performer with all the essential entity-types such as activity, role, application, and relevant data. The Fig. 1 illustrates these performer-centered affiliation relationships in a specific ICN-based workflow model. We are particularly interested in the performer-activity affiliation relationships in a workflow model, where the performers (or actors) are linked in activities through joint participations; reversely, the activities are connected to performers through joint involvements; the authors' research group has modeled a collection of these participations and involvements as "*workflow-supported performer-activity affiliation network model*[6][7]."

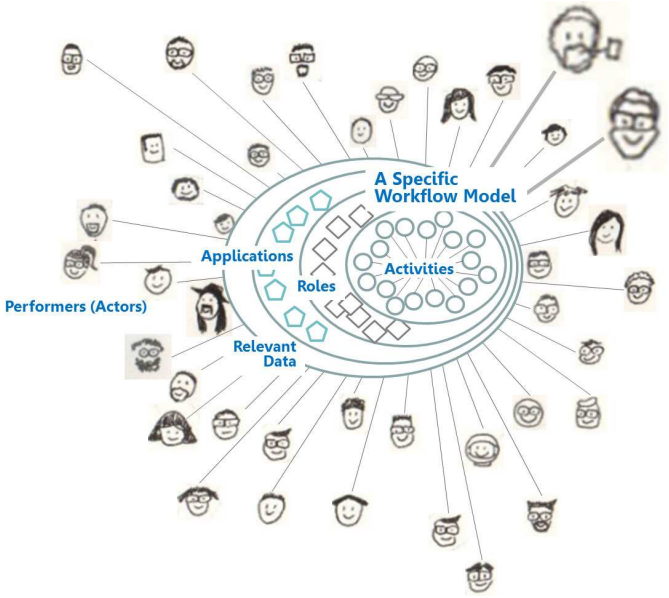

Fig. 1. Four Types of the Performer-Centered Affiliation Relationships in an Information Control Net of Workflow Model

In this paper, we focus on quantitatively measuring the degree of performers' familiarity by adopting the concept of closeness centralities into the workflow-supported performer-

Manuscript received September 27, 2016. This work is a follow up of the accepted conference paper as an outstanding paper in the 15th IEEE International Conference on Advanced Communications Technology. This research was supported by Basic Science Research Program through the National Research Foundation of Korea(NRF) funded by the Ministry of Education, Science and Technology (Grant No. 2012006971).

Hyunah Kim is with the department of computer science, Kyonggi University, 154-42 Kwangkyosan-ro Youngtong-gu Suwon-si Gyeonggi-do, 16227, Republic of Korea (e-mail: hyuna2486@naver.com)

Kwanghoon Pio Kim is with the collaboration technology research laboratory in the department of computer science, Kyonggi University, 154-42 Kwangkyosan-ro Youngtong-gu Suwon-si Gyeonggi-do, 16227, Republic of Korea (correponding author, phone: +82-31-249-9679, fax: +82-31-249-8949, e-mail: kwang@kgu.ac.kr)

activity affiliation network model. We assume that a workflow-supported performer-activity affiliation network is formed by two key groups of the entity types such as a set of performers and a collection of activities in a corresponding information control net of workflow model. That is, we are basically concerned about numerically formalizing the closeness centralities among the performers involved in fulfilling the ICN-based workflow model. Basically, the affilation network is coming from the formal properties[8]—two-mode and non-dyadic networks—of affiliation relationships. Since the workflow-supported performer-acitivity affiliation network is a two-mode network, the complete measurements should be done by giving centrality indices for both performers and activities. Generally, there are four centrality analysis techniques, such as degree, closeness, betweenness, and eigenvector centralities, and we particularly measure the closeness centralities of performers and the closeness centralities of activities in this paper.

By analyzing the closeness centralities on a workflow-supported performer-activity affiliation network formed from a set of activity-performer affiliated relationships in an ICN-based workflow model, it is eventually possible to visualize and numerically express how much the performers and the activities are interrelated and collaboratively closed in enacting the corresponding workflow model. As a consequence, the main purpose of this paper is to theoretically develop formulations and their algorithms for calculating the closeness centralities for activities and performers in a 'workflow-supported performer-activity affiliation network. In the next section, we simply describe the basic concept of the workflow-supported performer-activity affiliation network through the formal definition and the graphical representation as well. And, in the consecutive section we try to formulate the closeness centrality equations and their implementation algorithms with an operational example. Finally, we finalize the paper with describing a couple of related works in the last section.

II. Workflow-Supported Performer-Activity Affiliation Network Model

In order to represent the workflow-supported performer-activity affiliation knowledge, [6] has recently defined a graphical (Bipartite Graph) and formal representation model, which is dubbed workflow-supported performer-activity affiliation network model, which is abbreviated to APANM, and it has two types of nodes—a set of performers and a set of activities—and a set of relationships between those nodal types. Thus a workflow-supported performer-activity affiliation network model is a two-mode network model with aiming to accomplish the following dual objectives:

- to uncover the relational structures of workflow-performers through their joint involvement in activities, and
- to reveal the relational structures of workflow-activities through their joint participation of common performers.

Additionally, those relational structures can be weighed to measure the extent of their strengths by assigning a value to each of relations between nodal types. Therefore, there are two types of performer-activity affiliation networks—binary performer-activity affiliation network and valued performer-activity affiliation network. In the binary performer-activity affiliation network, its value (0 or 1) implies a binary relationship of involvement (or participation), while values in the valued performer-activity affiliation network may represent various implications according to their application domains; typical examples of values might be stochastic (or probabilistic) values, strengths, and frequencies. The formal knowledge representation of workflow-supported performer-activity affiliation network model is defined in the following [Definition 1][6].

[Definition 1] Workflow-Supported Performer-Activity Affiliation Network Model. A workflow-supported performer-activity affiliation network model is formally defined as $\Lambda = (\sigma, \psi, \mathbf{S})$, over a set $\mathbf{C}$ of performers (actors), a set $\mathbf{A}$ of activities, a set $\mathbf{V}$ of weight-values, a set $\mathbf{E}_p \subseteq (\mathbf{C} \times \mathbf{A})$ of edges (pairs of performers and activities), and a set $\mathbf{E}_a \subseteq (\mathbf{A} \times \mathbf{C})$ of edges (pairs of activities and performers), where, $\wp(\mathbf{A})$ represents a power set of the activity set, $\mathbf{A}$:

- $\mathbf{S}$ is a finite set of work-sharing actors or groups of some external performer-activity affiliation network models;
- $\sigma = \sigma_p \cup \sigma_v$ /* Involvement Knowledge */
  where, $\sigma_p : \mathbf{C} \longrightarrow \wp(\mathbf{A})$ is a single-valued mapping function from a performer to its set of involved activities;
  $\sigma_v : \mathbf{E}_p \longrightarrow \mathbf{V}$ is a single-valued mapping function from an edge $(\in \mathbf{E}_p)$ to its weight-value;
- $\psi = \psi_a \cup \psi_v$ /* Participation Knowledge */
  where, $\psi_a : \mathbf{A} \longrightarrow \wp(\mathbf{C})$ is a single-valued mapping function from an activity to a set of participated performers; and $\psi_v : \mathbf{E}_a \longrightarrow \mathbf{V}$ is a single-valued function from an edge $(\in \mathbf{E}_a)$ to its weight-value;

Furthermore, the affiliation knowledge representation can be graphically depicted by an affiliation graph. So, a workflow-supported performer-activity affiliation network's graphical model consists of two types of graphical nodes—a set of performers (shaped in hexagon) and a set of workflow activities (shaped in circle)—and a set of non-directed edges between two nodal types, which means that a workflow affiliation network is a non-directed graph. That is, in a workflow-supported performer-activity affiliation graph, non-directed lines connect performers aligned on one side of the diagram to the workflow activities aligned on the other side. Importantly, a performer-activity affiliation graph does not permit lines among the performers nor among the workflow activities. Therefore, a performer-activity affiliation graph with g performers and h workflow activities can be transformed into a matrix with 2-dimension of $g \times h$.

III. Closeness Centrality Measurement Formulations

In general, an affiliation networking graph[9] is a bipartite graph, as described in the previous section, in which non-directed lines connect performers aligned on one side of the diagram to the workflow activities aligned on the other side.

Based upon the performer-activity affiliation networking graph and its affiliation matrix, it is possible to analyze a variety of knowledge analytics issues[9], such as mean rates analysis[8], density measurements[8], and centrality measurements[9], raised from the social networking literature. In this paper, our focus concentrates upon the centrality measurements of the workflow-supported affiliation network model. More precisely speaking, we try to propose an algorithmic formalism for analyzing organizational centrality measurements, particularly closeness centrality measurements, of a workflow-supported performer-activity affiliation network.

A. Definition of Affiliation Matrix

Eventually, it is necessary for the performer-activity affiliation network model to be analyzed in a mathematical representation. A workflow-supported performer-activity affiliation network model is graphically represented by a bipartite graph, and at the same time it is mathematically represented by an affiliation matrix. The affiliation matrix can be realized by either an involvement matrix or a participation matrix. That is, a performer-activity affiliation network model is mathematically transformed into an activity-performer affiliation matrix that records the presence and absence of g performers at h workflow activities; thus its dimensions are g rows and h columns, respectively. If a certain performer ϕ_i attends a workflow activity α_j, then the entry in the i^{th} and j^{th} cell in the matrix equals to 1; otherwise the entry is 0. Denoting a binary activity-performer affiliation matrix as $\mathbf{Z}$, its $x_{i,j}$ values meet these conditions:

$$x_{i,j} = \begin{cases} \mathbf{1} & \textit{if performer}, \phi_i, \textit{is affiliated with activity}, \alpha_j \\ \mathbf{0} & \textit{otherwise} \end{cases} \tag{1}$$

- The row total, also called row marginals, ($\overline{D}_r$), of a performer-activity affiliation matrix $\mathbf{Z}$ sum to the number of workflow activities that each performer will attend, which implies the involvement relations between activities and performers in a specific workflow model.

$$\overline{D}_r = \left[\sum_{j=1}^{h} x_{i,j} \right]_{i=1}^{g} \tag{2}$$

- The column marginals, ($\overline{D}_c$), indicate the number of performers who will attend each workflow activity's enactment, which implies the participation relations between performers and activities in a corresponding workflow model.

$$\overline{D}_c = \left[\sum_{i=1}^{g} x_{i,j} \right]_{j=1}^{h} \tag{3}$$

Also, assuming an affiliation networking graph has g performers and h activities, then its bipartite affiliation matrix has dimensions $(g + h) \times (g + h)$. Consequently, using the involvement affiliation matrix ($\mathbf{Z}_p$) and the participation affiliation matrix ($\mathbf{Z}_a$) forms an affiliation bipartite matrix, $\mathbf{X}^{P,A}$, which can be schematically represented as the following equations, (4) and (5).

$$\mathbf{X}^{P,A} = \begin{bmatrix} \mathbf{0} & \mathbf{Z}_p \\ \mathbf{Z}_a & \mathbf{0} \end{bmatrix} \tag{4}$$

$$\mathbf{X^P} = \mathbf{Z_p} \cdot \mathbf{Z_a} \qquad \mathbf{X^A} = \mathbf{Z_a} \cdot \mathbf{Z_p}; \tag{5}$$

B. Closeness Centrality Formulations

[8] gives a series of well-described equations that can be applied to calculating the closeness centralities based upon the bipartite matrix of a workflow-supported performer-activity affiliation network model. Before we develop an algorithm of the closeness centrality measurements in the next subsection, we need to restate those closeness centrality equations, and consider the relationship between the closeness centrality of a performer and the closeness centrality of the activities to which the performer belongs, and the relationship between the closeness centrality of an activity and the closeness centrality of its performers.

Basically, the meaning of closeness centrality index in a social network[1][3] implies the average geodesic distance that a node is from all other nodes in the graph. In other words, it is to calculate the 'farness' of a node from other nodes in the graph. As described in the previous section, the performer-activity affiliation network is a special type of social network, and it is represented by a bipartite graph with relationships (or connections) between performers and activities. Thus, calculating the geodesic distances in a bipartite graph begins with a function of the distances from the activities to the performers which each of them belongs. The distance from a node i representing a performer to any node j (either performer or activity) is $d(i,j) = 1 + \min\{d(k,j)\}_k$, for every activity node k adjacent to i. Given this properties, the closeness centrality of a performer in the bipartite graph can be expressed with a function of the distances from the performer's activities, k:

$$\sum_{j=1}^{g+h} d(i,j) = \sum_{j=1}^{g+h} \left[1 + \min\{d(k,j)\}_k\right], i \neq j \tag{6}$$

1) Closeness Centrality of Performers: Based on the distance function of (6), the following expressions are the index and the standardized index of the closeness centrality of a performer with a function of the minimum geodesic distances from its activities to other actors and to other activities, respectively. Note that every activity n_a is adjacent to performer n_i.

- The Index of Closeness Centrality of Performers

$$OC_C(n_i) = \left[\sum_{j=1}^{g+h} d(i,j) \right]^{-1} \quad (i \neq j) \tag{7}$$

$$OC_C(n_i) = \left[1 + \sum_{j=1}^{g+h} \min\{d(n_a, n_j)\}_a \right]^{-1} \quad (i \neq j) \tag{8}$$

- The Normalized Index of Closeness Centrality of Performers

$$OC_C^S(n_i) = (g + h - 1) \cdot [OC_C(n_i)] \tag{9}$$

$$OC_C^S(n_i) = \left[1 + \frac{\sum_{j=1}^{g+h} \min\{d(n_a, n_j)\}_a}{g+h-1}\right]^{-1} \quad (i \neq j) \tag{10}$$

2) Closeness Centrality of Activities: By revising the distance function of (6), it is also necessary to make the expressions for the index and the standardized index of the closeness centrality of an activity with a function of the minimum geodesic distances from its performers to other activities and to other performers. Note that every performer m_p is adjacent to activity m_j.

- The Index of Closeness Centrality of Activities

$$OC_C(m_i) = \left[1 + \sum_{j=1}^{g+h} \min\{d(m_p, m_j)\}_p\right]^{-1} \quad (i \neq j) \tag{11}$$

- The Normalized Index of Closeness Centrality of Activities

$$OC_C^S(m_i) = \left[1 + \frac{\sum_{j=1}^{g+h} \min\{d(m_p, m_j)\}_p}{g+h-1}\right]^{-1} \quad (i \neq j) \tag{12}$$

Summarily speaking, the equations (9) and (12) are for normalizing the index of closeness centrality by multiplying by $(g+h-1)$. Suppose that a performer is close to all others, which means that its adjacent activity has a direct tie to every performer in the bipartite graph. Thus the computed index values will be vary according to their graph sizes. In order to control the size of the graph, it is necessary for the individual index to be normalized so as to allow meaningful comparisons of performers across different graphs. This explanation can be identically applied to the normalized index for activities.

C. Algorithms of the Geodesic Distances

Based upon those closeness centrality equations, we develop a series of algorithms for calculating the closeness centralities of all the performers as well as all the activities associated with a workflows-supported performer-activity affiliation network. The following subsections concisely describe the details of the algorithms and their explanations. Note that we won't put all the algorithms that are needed to calculate the closeness centralities.

1) Algorithm of the geodesic distances for performers: By extensively applying the equations of (8) and (10), we can calculate the closeness centralities of performers for a workflow-supported performer-activity affiliation network. The essential part of those equations must be the functions of calculating the geodesic distance from a performer node, n_i, to another performer node, n_j, and the geodesic distance, which implies the shorted path, from a performer node, n_i, to an activity node, m_j, respectively. In this subsection, we devise an algorithm with recursive functions, to algorithmically implement the essential equations. Assume that the algorithm operates on a given performer-activity affiliation adjacency matrix, $\mathbf{X}^{P,A}$, representing the corresponding workflow-supported performer-activity affiliation network, and its functional procedure name is 'PcGeodesicDistance()' using two recursive functions, 'gDistance()' and 'hDistance()', which are calculating the geodesic distances from a specified performer (n_i) to all the performers and to all the activities, respectively. The output of the algorithm is the geodesic distance of a performer, n_i, to either a performer or an activity, n_j, and it is saved on the performer-centered geodesic distance matrix, $\mathbf{G}^{P,A}$, as a value of the cell, $\mathbf{G}^{P,A}[n_i, n_j]$. The time complexity of the algorithm is $\mathbf{O}(\mathsf{N})$, where $\mathsf{N} = g+h-1$, and g is the number of performers and h is the number of activities in a corresponding workflow-supported performer-activity affiliation network.

The Geodesic Distances Algorithm for Performers:

01: **Given Global** A Binary Affiliation Bipartite Matrix, $X^{P,A}[g+h, g+h]$;
02: **Given Global** A Set of Performers, **P**;
03: **Given Global** A Set of Activities, **A**;

04: **Procedure Name: PcGeodesicDistance**
05: **Input** A Performer (From), n_i;
06: Either a Performer or an Activity (To), n_j;
07: **Output** A Performer-Centered Geodesic Distance Measure, $G^{P,A}[n_i, n_j]$;

08: **Local** An Activity Distance Vector, $G_k[1..h]$, initialized by **maximum**;
09: **Local** A Performer Distance Vector, $H_k[1..g]$, initialized by **maximum**;

10: **Begin Procedure**
11: **If** ($n_j \in \mathbf{P} \wedge n_i \neq n_j$)
12: **For** ($\forall m_k \in \boldsymbol{A}_k$ *adjacent to* n_i)
13: $G_k[m_k] \leftarrow$ **gDistance**(n_i, m_k, n_j);
14: **roF**
15: $G^{P,A}[n_i, n_j] \leftarrow 1 +$ **minimum**$\left(G_k[i]\right)_{i=1}^{h}$;
16: **Else If** ($n_j \in \mathbf{A}$)
17: **For** ($\forall m_k \in \boldsymbol{A}_k$ *adjacent to* n_i)
11: **If** ($m_k = n_j$)
11: $G_k[m_k] \leftarrow 0$; **break**;
20: **Else If** ($m_k \neq n_j$)
21: $\mathbf{P}_s \leftarrow$ all performers who are adjacent to m_k;
22: $\mathbf{P}_s \leftarrow \mathbf{P}_s - n_i$;
23: **For** ($\forall n_s \in \boldsymbol{P}_s$)
24: $H_k[n_s] \leftarrow$ **hDistance**(m_k, n_s, n_j);
25: **roF**
26: $G_k[m_k] \leftarrow 1 +$ **minimum**$\left(H_k[i]\right)_{i=1}^{g}$;
27: **Initialize** $H_k[1..g]$ by **maximum**;
28: **roF**
29: $G^{P,A}[n_i, n_j] \leftarrow 1 +$ **minimum**$\left(G_k[i]\right)_{i=1}^{h}$;
30: **Return** $G^{P,A}[n_i, n_j]$;
31: **End Procedure**

2) Algorithm of the Geodesic Distance for Activities: We develop an algorithm for implementing the above equations of (11) and (12) by revising the algorithm developed in the previous subsection. By using the algorithm we are able to calculate the closeness centralities from a activities' point of view. Likewise, the essential part of those equations must be the functions of calculating the geodesic distance from an activity node, m_i, to another activity node, m_j, and the geodesic distance from an activity node, m_i, to a performer node, n_j, respectively. Assume that the algorithm also operates on a given performer-activity affiliation adjacency matrix, $\mathbf{X}^{P,A}$, representing the corresponding workflow-supported performer-activity affiliation network, and its functional procedure name is 'AcGeodesicDistance()' using two recursive functions, 'gDistance()' and 'hDistance()', too. The output of the algorithm is the geodesic distance measure of an activity, m_i, to either a performer or an activity, m_j, and it is saved on the activity-centered geodesic distance matrix, $\mathbf{G}^{P,A}$, as a value of

the cell, $\mathbf{G}^{A,P}[m_i, m_j]$. The time complexity of the algorithm is $\mathbf{O}(\mathsf{N})$, where $\mathsf{N} = g + h - 1$, and g is the number of performers and h is the number of activities in a corresponding workflow-supported performer-activity affiliation network.

The Geodesic Distances Algorithm for Activities:

Given Global A Binary Affiliation Bipartite Matrix, $X^{P,A}[g + h, g + h]$;
Given Global A Set of Performers, **P**;
Given Global A Set of Activities, **A**;

Procedure Name: AcGeodesicDistance
Input An Activity (From), m_i;
Either an Activity or a Performer (To), m_j;
Output An Activity-Centered Geodesic Distance Measure, $G^{A,P}[m_i, m_j]$;

Local A Performer Distance Vector, $H_k[1..g]$, initialized by **maximum**;
Local An Activity Distance Vector, $G_k[1..h]$, initialized by **maximum**;

Begin Procedure
  If ($m_j \in \mathbf{A} \wedge m_i \neq m_j$)
    For ($\forall n_k \in \boldsymbol{P}_k$ *adjacent to* m_i)
      $H_k[n_k] \leftarrow$ **hDistance**(m_i, n_k, m_j);
    roF
    $G^{A,P}[m_i, m_j] \leftarrow 1 +$ **minimum**$\left(H_k[i]\right)_{i=1}^{g}$;
  Else If ($m_j \in \mathbf{P}$)
    For ($\forall n_k \in \boldsymbol{P}_k$ *adjacent to* m_i)
  If ($n_k = m_j$)
      $H_k[n_k] \leftarrow 0$; **break**;
    Else If ($n_k \neq m_j$)
      $\mathbf{A}_s \leftarrow$ all activities that are adjacent to n_k;
      $\mathbf{A}_s \leftarrow \mathbf{A}_s - m_i$;
      For ($\forall m_s \in \boldsymbol{A}_s$ *adjacent to* n_k)
        $G_k[m_s] \leftarrow$ **gDistance**(n_k, m_s, m_j);
      roF
      $H_k[n_k] \leftarrow 1 +$ **minimum**$\left(G_k[i]\right)_{i=1}^{h}$;
      Initialize $G_k[1..h]$ by **maximum**;
    roF
    $G^{A,P}[m_i, m_j] \leftarrow 1 +$ **minimum**$\left(H_k[i]\right)_{i=1}^{g}$;
  Return $G^{A,P}[m_i, m_j]$;
End Procedure

D. Implications of the Closeness Centralities

In this paper, we are particularly interested in adopting the concept of closeness centrality to measure *the degree of familiarity* among performers in a workflow-supported orgranization. The semantic significance of closeness distance in terms of the familiarity metric refers to how quickly a performer can interact with others via intermediary activities where the performers are jointly participating to. In consequence of those consecutive calculations of all the performers, we can draw the answers to the following question from measuring the closeness centralities on a workflow-supported performer-activity affiliation network:

- **The degree of familiarity**: How quickly can a performer interact with others *via* very few intermediary activities in enacting workflow procedures?

Conclusively, the answer to the question is able to convey a very valuable and meaningful insight to the corresponding workflow-supported organization. We assure that the primary rationale of the closeness centrality ought to be on the question and the answer. We strongly believe that a series of theoretical formulations on the closeness centralities and their implementable algorithms devised in this paper can be used in developing a workflow-supported organizational intelligent system supporting to measure the individual levels as well as the group levels of the closeness centralities in a workflow-supported organization.

IV. Related Works

Recently, technology-supported social networks and organizational behavioral analytics issues have been raised in the IT literature. Naturally, the workflow literature has just started transitioning into and focusing on social and collaborative work analyses in workflow-supported organizations, because workflow management systems are "human systems," where workflow procedures must be designed, deployed, and understood within their social and organizational contexts. It is quite natural for the concept of enterprise social networks (workflow-supported affiliation networks) to be raised and issued from these human-centered organizational contexts. It is important to remind that the human-centered affiliation relationships reveal how each of the individuals is associated with the essential entity-types of the organizational resources like activity, role, application, and relevant data. Particularly, in this paper we focus on the Performer-Activity affiliation networking knowledge[7] and fomulate their equations for calculating the closeness centralities among the performers.

K. P. Kim [7] firstly issued the workflow-supported performer-activity affiliation network as a special type of organizational social network knowledge acquired from deploying workflow technologies. In the paper, the author theoretically derived a series of concepts and algorithms not only for representing and discovering those knowledge but also for analyzing the discovered knowledge. Battsetseg, *et al*. [10] proposed a theoretical formalism to analyze a workflow-supported performer-activity affiliation network by measuring the organizational closeness centralities of performers as well as the organizational closeness centralities of activities. Note that we try to extend the proposed theoretical formalisms through this paper. H. Kim, *et al*. [11] formalized the workflow-supported performer-role affiliation network. In the paper, the authors formally defined the workflow-supported performer-role affiliation networking knowledge through a series of theoretical formalisms and practical implementation for modeling, discovering, and visualizing workflow performer-role affiliation networking knowledge. H. A. Reijers, *et al*. [12] pioneered the human-centered resource management issue in a workflow-suppoted organization, which can be interpreted by a conceptual species of the workflow-supported affiliation networks. Through this research, they showed that the high degree of geographical closenesses among workflow-performers be leaded to the posivitve effect on workflow-supported organizational performance by conducting a case study of distributed teamworks on a workflow process model.

Conclusively, we would say that these pioneering works, until now, concerning about the human-centered affiliation knowledge are the outputs in the stage of initiative research works, which is the discovery phase. The next stage ought to be the analysis phase. The paper of [10] was just a halffinished step forward to the analysis phase shifting from the discovery

phase. In particulay, P. Busch and his colleague in [13][14] raised the logical necessity of the conceptual triangulation of workflow management, social network analysis, and knowledge management, which ought to be one of the circumstantial evidences of the theoretical importance of this paper.

V. Conclusion

In this paper, we have formulated a series of closeness centrality measurement equations and proposed their related algorithms and descriptions for analyzing a workflow-supported performer-activity affiliation network representing involvement and participation behaviors between workflow-based people and workflow-based activities. We have introduced the basic concept of workflow-supported performer-activity affiliation network and its implications as a meaningful mechanism of organizational knowledge and intelligence. Particularly, we restate the mathematical equations for the closeness centrality measurements, and develop an functional algorithm for implementing those closeness centrality equations. As a future work, we have a plan to implement those concept and algorithms for measuring the closeness centralities as a fundamental function of the organizational knowledge and intelligent management system.

Acknowledgment

This research was supported by Basic Science Research Program through the National Research Foundation of Korea(NRF) funded by the Ministry of Education, Science and Technology (Grant No. 2012006971).

References

[1] W. M. P. van der Aalst, H. A. Reijers, and M. Song, "Discovering social networks from event logs," *Computer Supported Cooperative Work*, vol. 14, no. 6, pp. 549–593, 2005.

[2] J. Won, "A framework: Organizational network discovery on workflows," Ph.D. dissertation, Kyonggi University, 2008.

[3] J. Song, M. Kim, H. Kim, and K. Kim, "A framework: Workflow-based social network discovery and analysis," in *Proceedings of the IEEE 13th International Conference on Computational Science and Engineering*, Hongkong, China, Dec. 2010, pp. 421–426.

[4] C. A. Ellis and G. J. Nutt, "Office information systems and computer science," *ACM Computing Surveys*, vol. 12, no. 1, pp. 27–60, 1980.

[5] K. Kim, "Actor-oriented workflow model," in *Proceedings of the 2nd international symposium on Cooperative Database Systems for Advanced Applications*, WOLLONGONG, AUSTRALIA, Mar. 1999, pp. 150–164.

[6] H. Kim, H. Ahn, and K. P. Kim, "A workflow affiliation network discovery algorithm," *ICIC Express Letters*, vol. 6, no. 3, pp. 765–770, 2012.

[7] K. P. Kim, "Discovering activity-performer affiliation knowledge on icn-based workflow model," *Journal of Information Science and Engineering*, vol. 29, pp. 79–97, 2013.

[8] D. Knoke and S. Yang, *SOCIAL NETWORK ANALYSIS - 2nd Edition, Series: Quantitative Applications in the Social Sciences*. SAGE Publications, 2008.

[9] K. Faust, "Centrality in affiliation networks," *Journal of Social Networks*, vol. 19, pp. 157–191, Aug. 1997.

[10] A. Battsetseg, H. Ahn, M. Park, H. Kim, W. Yoon, and K. P. Kim, "Organizational closeness centrality analysis on workflow-supported activity-performer affiliation networks," in *Proceedings of the IEEE 13th International Conference on Advanced Communications Technology*, Phoenix Park, Pyeongchang, South Korea, Feb. 2013.

[11] H. Kim, H. Ahn, and K. P. Kim, "Modeling, discovering, and visualizing workflow performer-role affiliation networking knowledge," *KSII Transactions on Internet and Information Systems*, vol. 8, no. 2, pp. 134–151, February 2014.

[12] H. A. Reijers, M. Song, and B. Jeong, "Analysis of a collaborative workflow process with distributed actors," *Information Systems Frontiers*, vol. 11, no. 3, pp. 307–322, 2009.

[13] E. Kim and P. Busch, "Workflow interpretation via social networks," *Lecture Notes on Artificial Intelligence*, vol. 9806, pp. 241–250, 2016.

[14] P. Busch, "Business process management, social network analysis and knowledge management: A triangulation of sorts?" in *Proceedings of the the 21st Australasian Conference on Informaiton Systems*, Brisbane, Austrailia, Dec. 2010.

Hyunah Kim Dr. Kim is an adjunctive professor and a faculty member of the collaboration technology research laboratory in the department of computer science at Kyonggi University, South Korea. She received her B.S. degree in computer science from Korea Nazarene University in 2001. Also, she received her M.S. and Ph.D. degrees in computer science from Kyonggi University in 2003 and 2009, respectively. She has been on the operational committees of several domestic and international conferences including KSII, AP-IST, ICONI, and ICACT. Her research interests include workflow systems, SCORM-based e-Learning process models, BPM, BPI, ACM, workflow-supported social networks discovery and analysis, and process-aware Internet of Things.

Kwanghoon Pio Kim Dr. Kim is a full professor of computer science department and the founder and supervisor of the collaboration technology research laboratory at Kyonggi University, South Korea. He received B.S. degree in computer science from Kyonggi University in 1984. And he received M.S. degree in computer science from Chungang University in 1986. He also received his M.S. and Ph.D. degrees from the computer science department at University of Colorado Boulder, in 1994 and 1998, respectively. He had worked as researcher and developer at Aztek Engineering, American Educational Products Inc., and IBM in USA, as well as at Electronics and Telecommunications Research Institute (ETRI) in South Korea. In present, he is a vice-chair of the BPM Korea Forum. He has been in charge of a country-chair (Korea) and ERC vice-chair of the Workflow Management Coalition. He has also been on the editorial board of the journal of KSII, and the committee member of the several conferences and workshops. His research interests include groupware, workflow systems, BPM, adaptive case management (ACM), CSCW, collaboration theory, Grid/P2P/Cloud distributed workflow systems, process warehousing and mining, workflow-supported social networks discovery and analysis, process-aware information systems, data intensive workflows, and process-aware Internet of Things.

Volume 5 Issue 6, Sep. 2016, ISSN: 2288-0003

ICACT-TACT JOURNAL

Global IT Research Institute

1713 Obelisk, 216 Seohyunno, Bundang-gu, Sungnam Kyunggi-do, Republic of Korea 13591

Business Licence Number : 220-82-07506, Contact: secretariat@icact.org Tel: +82-70-4146-4991